MATHEMATICAL MODELING AND SIMULATION OF SUSPENSION
DROPLET DRYING

A THESIS SUBMITTED TO
THE GRADUATE SCHOOL OF NATURAL AND APPLIED SCIENCES
OF
MIDDLE EAST TECHNICAL UNIVERSITY

BY

AHMET FURKAN ÖZCAN

IN PARTIAL FULFILLMENT OF THE REQUIREMENTS
FOR
THE DEGREE OF MASTER OF SCIENCE
IN
CHEMICAL ENGINEERING

SEPTEMBER 2019

Approval of the thesis:

MATHEMATICAL MODELING AND SIMULATION OF SUSPENSION DROPLET DRYING

submitted by **AHMET FURKAN ÖZCAN** in partial fulfillment of the requirements for the degree of **Master of Science in Chemical Engineering Department, Middle East Technical University** by,

Prof. Dr. Halil Kalıpçılar
Dean, Graduate School of **Natural and Applied Sciences**   _____

Prof. Dr. Pınar Çalık
Head of Department, **Chemical Engineering**   _____

Prof. Dr. Yusuf Uludağ
Supervisor, **Chemical Engineering, METU**   _____

Examining Committee Members:

Prof. Dr. Halil Kalıpçılar
Chemical Engineering, METU   _____

Prof. Dr. Yusuf Uludağ
Chemical Engineering, METU   _____

Assoc. Prof. Dr. Erhan Bat
Chemical Engineering, METU   _____

Asst. Prof. Dr. İnci Ayrancı Tansık
Chemical Engineering, METU   _____

Assoc. Prof. Dr. Berna Topuz
Chemical Engineering, Ankara University   _____

Date: 06.09.2019

I hereby declare that all information in this document has been obtained and presented in accordance with academic rules and ethical conduct. I also declare that, as required by these rules and conduct, I have fully cited and referenced all material and results that are not original to this work.

Name, Surname: Ahmet Furkan Özcan

Signature:

ABSTRACT

MATHEMATICAL MODELING AND SIMULATION OF SUSPENSION DROPLET DRYING

Özcan, Ahmet Furkan
Master of Science, Chemical Engineering
Supervisor: Prof. Dr. Yusuf Uludağ

September 2019, 109 pages

Drying procedures like spray drying, fluidized bed drying etc. are widespread industrial applications. Such procedures mainly aim to produce high value pharmaceuticals and bulk commodities such as dried milk and detergent powders, which require controlled physical properties that are dependent on the drying process that they are subject to. The aim of this study is to model the kinetics of water droplet drying containing nanosized SiO_2 particles and simulate the coupled heat and mass transfer processes via a computer program.

The main physical mechanisms involve initial transfer of heat by convection from flowing air with constant properties and then thermal conduction and evaporation of water from the liquid interface, simultaneous diffusion of liquid and nanoparticles leading to agglomeration of solid particles near liquid interface and eventually formation of a shell structure, while a shrinkage in droplet size occurs. As the wet shell region widens with adhering nanoparticles from the inner region, at a certain point shell strength becomes able to sustain the capillary forces exerted by receding water and consequently solid particles in the shell region ceases to recede. Beyond this point, liquid interface recedes towards the center as water evaporation still continues through

the pores of the dry crust region, which was a part of former wet shell itself. On the other hand, transfer diffusion of water molecules at the center of the particle towards the evaporation front causes a vacant region to form in the middle, provided that initial amount of solid particles is not sufficient to fill the entire volume of the dried structure. The essential focus in this study is on the kinetics of suspension droplet drying after the liquid interface recedes behind solid particles, namely the dry crust. Eventually all water molecules evaporate from the inner region of the particle leading to either a solid or hollow particle morphology depending on the initial solid fraction.

ÖZ

SÜSPANSİYON TANECİĞİ KURUMASININ MATEMATİKSEL MODELLEMESİ VE SİMÜLASYONU

Özcan, Ahmet Furkan
Yüksek Lisans, Kimya Mühendisliği
Tez Danışmanı: Prof. Dr. Yusuf Uludağ

Eylül 2019, 109 sayfa

Sprey kurutması, akışkan yataklı kurutma vb. kurutma prosedürleri yaygın olarak kullanılan endüstriyel uygulamalardır. Bu tür uygulamalar, kurutma sürecinin fiziksel şartlarına bağlı olan ve bu şartların üretim sürecinde kontrol edilebilir olmasına gerek duyan deterjan tozu ve kurutulmuş süt gibi farmasötik ve toplu halde üretilen ürünlerin üretimini amaçlamaktadır. Bu çalışmanın amacı nano ölçekte SiO_2 partikülleri içeren su damlacığının kuruma kinetiğinin modellenmesi ve birbirine bağlı ısı ve kütle transferi süreçlerinin bilgisayar programı yardımıyla simüle edilmesidir.

Kuruma süreci boyunca gerçekleşen ana fiziksel mekanizmalar genel olarak, ısının öncelikle sabit özelliklere sahip bir hava akımı konveksiyonu ile sonra da kondüksiyon ile parçacığın iç kısmına iletimi ve suyun sıvı yüzeyinden buharlaşması, eş zamanlı olarak buharlaşmadan dolayı damlacık boyutu küçülürken sıvı moleküllerin katı partiküllerle beraber difüzyonu ve bunun sonucunda sıvı yüzeyinde katı madde birikmesi sonucu bir kabuk yapısının oluşması olarak özetlenebilir. Islak kabuk yüzeyi iç yüzeyden yapışan partiküllerle genişlerken, bir noktadan sonra kabuk yapısı geri çekilen su moleküllerinin oluşturduğu kapiler kuvvete dayanabilir hale gelir ve kabuk yüzeyinin geri çekilmesi sona erer. Bu aşamadan sonra su yüzeyi buharlaşmanın etkisiyle merkeze doğru geri çekilmeye devam ederken, merkezdeki

su molekülleri de buharlaşma yüzeyine doğru transfer difüzyonuna uğrar ve ilk andaki katı miktarının parçacık hacmini tamamen dolduramayacağından dolayı parçacığın iç tarafında boşluklu bir yapının oluşmasına sebep olur. Bu çalışmada odak noktası süspansiyon damlacığın sıvı yüzeyi katı partiküllerin gerisine çekildikten sonraki süreçteki kuruma kinetiği olacaktır. Nihayetinde parçacıkta bulunan tüm su molekülleri buharlaşır ve ilk durumdaki katı miktarına bağlı olarak tam dolu ya da boşluklu bir parçacık morfolojisi elde edilir.

Anahtar Kelimeler: Nanosüspansiyon, Kuruma, Buharlaşma, Modelleme, Simülasyon

To my beloved parents, Aysın and Hasan

ACKNOWLEDGEMENTS

TABLE OF CONTENTS

LIST OF TABLES

TABLES

LIST OF FIGURES

FIGURES

xiv

LIST OF ABBREVIATIONS

ABBREVIATIONS

AH   Absolute humidity, g/g air

c   Concentration, mol/m^3

cp   Heat capacity, kJ/K

d   Diameter, m

D   Diffusivity, cm^2/s

h   Convective heat transfer coefficient, W/m^2K

J   Flux, kg/m^2s

k   Heat conductivity, W/mK

k_m Mass transfer coefficient, m/s

M   Molecular weight, kg/mol

N   Molar flux, mol/m^2s

Nu   Nusselt number

P   Pressure, atm

Pr   Prandtl number

q   Heat flux, W/m^2

R   Radius, m

Re   Reynolds number

R_g Gas constant, J/Kmol

Sc   Schmidt number

Sh   Sherwood number

t   Time, s

T   Temperature, K

v   Velociy, m/s

V   Volume, m^3

SUBSCRIPTS

a   Air

cr   Crust

d   Droplet

i   Initial

liq   Liquid

p   Particle

s   Solid

sh   Shell

sl   Slurry

v   Vapor

vap   Vaporization

vc   Vacancy

w   Water

wv   Water vapor

LIST OF SYMBOLS

SYMBOLS

ε Porosity

λ Latent heat of evaporation, kJ/kg

μ Viscosity, kg/ms

ρ Density, kg/m^3

φ Volume fraction

CHAPTER 1

INTRODUCTION

Drying operations such as spray drying, fluidized bed drying etc. take place broadly in industrial applications, mainly in chemical, pharmaceutical, food industries and many others. Many commercial products as bulk commodities are obtained as end product. However, such drying processes require certain operating conditions in order to meet desired properties for these products. Therefore, many experiments and researches are made to determine the optimal and feasible operation conditions and they are available in the literature.

Throughout the drying operation, the governing physical mechanisms are basically transfer of heat from ambient air and simultaneous evaporation and transfer of water molecules. Heat is initially received from ambient air by convection, and then further transmitted to the inner regions of the suspension droplet by conduction. At the same time, evaporation from water interface occurs and that results a reduction in droplet size until a certain point where solid particles cease receding together with evaporating water interface.

The overall drying process of a nano-suspension droplet can be generally investigated in two stages. First stage of evaporation, in other words constant rate of evaporation, involves the evaporation of water molecules from the outer surface of the droplet. Since there is no hindrance to mass and heat transfer in this stage, the rate of evaporation is constant until water interface recedes behind the solid particles present

in the slurry. This stage can also be considered as free evaporation of a droplet. Throughout the evaporation process in first stage, fraction of solid particles in the droplet constantly increases. This leads to a tighter formation of solid particles, on the other hand uniformity begins to be disrupted. Since evaporation of liquid occurs relatively fast, solid particles fail to preserve uniformity throughout the droplet resulting to agglomeration of particles in a region close to water-air interface. After some time the outermost water molecules align with the solid particles inside, as the solid particles begins to form a shell, in which they are in very tight formation, locked to each other with minimum porosity at the interface. From this point on evaporation mechanism continues as it is, nevertheless additional phenomena are introduced to receding mechanism of the droplet. Besides, this phase is also called as transition stage, which is a temporary phase within first drying stage and initiated with the formation of very first thin line of the shell region.

Although the droplet interface now includes both liquid and solid particles together, constant rate of evaporation is not affected from formed shell. As water is evaporating from the surface, solid particles also recede back with receding water interface. Initially an infinitesimal layer of water is present at droplet surface, therefore the water molecules at interface undergoes a free evaporation process. After a very short time interval, water interface falls behind the solid particles' outermost linage, where capillary forces come into play. Falling behind spherical solid particles creates surface menisci, which also enables capillary forces exerted by water to pull solid particles back with moving water interface. Afterwards, as solid particles recede back sufficiently, an infinitesimal water layer of water again emerges at droplet surface. However, these subsequent steps occur very rapidly, so that the whole receding process of the shell region, i.e. water and solid particles together with maximum solid fraction, can be considered as a simultaneous process. This concept is elaborately explained in Mezhericher et al [1].

Throughout the transition phase, more and more solid particles adhere to the shell inner boundary as a result of agglomeration, thus thickness of the shell region increases. Free evaporation of water from the surface continues until shell thickness reaches a certain point, so that the shell strength is capable to withstand against the capillary forces exerted by receding water interface. Time interval that shell would sustain thickening depends on many parameters such as strength of solid material, volume fraction of solid particles in shell region, emerging capillary forces by liquid etc. The point is that after some time solid particles remain stationary and determine the final outer diameter of the droplet. On the other hand, water recedes behind the solid particles due to the evaporation. At that point, first stage of evaporation comes to an end and so does the transition stage, at the same time the second stage of evaporation, in other words falling rate of evaporation begins.

This study mainly focuses on the second stage of evaporation, just after water molecules fall behind solid particles, which are stationary from this point on. In this stage, new hindrances are introduced to heat and mass transfer inside the droplet. Heat introduced to droplet now has to take a longer way through the porous matrix filled with water vapor, which is also called as dry crust, to reach the water interface. Additionally, evaporated water vapor molecules have to diffuse a longer way through the dry crust to reach the droplet surface. Therefore, evaporation rate decreases as water interface recedes further towards the center of the droplet.

The final particle morphology is determined at this point, since the outermost solid particles remain stationary. One of the important criteria is volume fraction of solid particles in innermost region, namely slurry region. This fraction value determines whether the final particle results in a hollow or fully solid particle. The main objective of this thesis work is further development of existing models and corresponding governing equations for both stages of single droplet drying, mostly focusing on the

second stage also with a detailed simulation of the process via COMSOL. Additionally, comparison and discussion of estimated results of the simulation are done among both individual studies and available data in literature. Further explanations and elaborate analysis of particle parameters and assumptions are introduced in modeling and simulation section.

CHAPTER 2

LITERATURE REVIEW

Evaporation of droplets and involved kinetics have been studied in detail and also experimented by many researchers with various theoretical approaches. Over the years, new models have been presented introducing additional mechanisms, related to either heat and mass transfer operations or morphological structure of the droplet. Furthermore, there have been also significant improvements in terms of experimental findings, which also result in additional concepts to come into play, such as surface forces at evaporating interface or emergence of a vacant region at the center etc. Although the models that are presented in the last 10-20 years have the potential to compile the evaporation kinetics of a droplet particle elaborately, it is also worth to take a look at former researches which provide a vital basis for later researches.

One of the first studies on kinetics of droplet evaporation was done by Ranz and Marshall [2], in which mechanism for heat and mass transfer operations for free evaporation process were investigated. Making use of these expressed correlations, Charlesworth and Marshall [3] took the line a step further by investigating the droplet behavior during evaporation process. The model presented was mainly focusing on the first stage with various assumptions such as spherical symmetry, constant droplet diameter, diffusion driven mass transfer of vapor to ambient air etc. Nevertheless, the predictions and experimental results reported by the authors were in considerable agreement.

An experimental and theoretical model was presented by Sano and Keey [4] including both first and second stages of evaporation. Internal concentration profiles were determined by using transient convective diffusion equations with additional terms. In that paper, it is also considered that a hollow region in the center of the droplet particle may arise which results in inflation or rupture of the particle. The coefficient for mass transfer was determined experimentally and described by a Fickian type of diffusion, whereas the droplet temperature was assumed uniform in both stages.

The model presented by Cheong et al. [5] introduces a two-stage evaporation where simultaneous heat and mass transfer rates are solved numerically. The continuous measurement was possible with an improved version of the technique introduced by Charlesworth and Marshall [3]. On the other hand hindrances to heat and mass transfer in subsequent time interval was neglected. Mass transfer mechanism was also similar to other papers, an effective diffusion coefficient of Fickian type. There was also a receding interface which moves towards the center as the evaporation process continues, separating wet and dry regions of the particle at the same time, which shows similarity also to current study in that aspect.

Nesic and Vodnik [6] presented a research on evaporation of droplets containing solid particles. A similar experimental procedure to Charlesworth and Marshall [3] was considered and experiments on evaporation kinetics were performed, which provided a basis for subsequent theoretical modeling studies. The stages of evaporation included in the model were described as initial heating and evaporation, quasi-equilibrium evaporation, crust formation and growth, boiling and finally porous particle drying, where their transition criteria were also defined. Fickian type diffusion was considered for moisture transfer and an energy conservation equation was developed for quasi steady state conditions. For the particles containing colloidal silica

and sodium sulphate, there was good agreement between the predicted and experimental data.

To predict the change in droplet mass and temperature Farid [7] presented a model for droplet drying containing solid particles. Similar to earlier reports, the droplet initially undergoes a heating process then shrinkage is introduced by evaporation, followed by crust formation. According to Farid's paper, the drying rate is mainly controlled by conduction resistances present inside the droplet and convection resistances introduced by ambient conditions. It is assumed that the temperature of the droplet is close to wet-bulb temperature of the air during the first stage of evaporation, whereas it shows an increase to the dry-bulb temperature of the air in the second stage. The predictions provided a good agreement with experimental data available in the literature.

Seydel et al. [8] focused on the development of the microscopic structure of solid particles in the droplet and a simulation of solid structure during the drying process was introduced. Contrary to previous models, population balance approach was utilized to model the distribution of the solid particles. The drying stages were however similar as initially free evaporation occurs from the surface followed by shell formation of the agglomerated solid particles and eventually either a dried hollow or solid particle or failure with burst or fracture. The results are discussed qualitatively regarding to numerical simulations.

A computational model for single droplet drying was presented by Dalmaz et. al. [9,10]. In these studies simultaneous heat and mass transfer mechanism and also receding evaporation interface approach was considered. Both stages of evaporation were studied with various assumptions implemented, some of those introducing certain

problematic conditions in exchange for morphological simplifications. Initially the droplet is assumed to be covered with watery region, which later on undergoes free evaporation. After the evaporation interface recedes back and the particle can be divided into two separate regions, namely dry crust and wet crust, and the second stage of evaporation begins. In the second stage evaporation occurs in the particle, under the dry crust region, in which the diffusion of water vapor is described with Fickian diffusion expression. The evaporation process is controlled by coupled heat and mass transfer operations. The model provides coupled partial differential equations describing heat and mass transfers. One of the major drawbacks in this study was the constant morphology assumption. Whereas the water interface recedes backwards towards the center, solid particles are assumed to be stationary, resulting in inconsistent predictions for the second stage. The validation of the developed model is done by a comparison with experimental results introduced by Nesic and Vodnik [6].

Few years ago Handscomb et al. [11,12,13] presented a couple of papers in this area. A new model involving population balance approach was considered for the drying kinetics of a droplet with suspended solids. [11] The model introduced two phases, which are an ideal binary solution containing solute and solvent, and a discrete phase with solid particles. Fickian diffusion was assumed for the mass transport of continuous phase with a volume averaged differential mass balance, whereas for discrete solid phase a population mass balance with non-uniform solid particles was introduced. Subsequent article of the authors extended their work as they have investigated the drying process of a droplet in the presence of a surface shell. [12] Concepts like shell thickening, dry shell, wet shell etc. were first introduced in this article. The proposed model with new structural assumptions was able to predict and demonstrate the properties such as final particle morphology, moisture profile and solid particle-size distribution. Further researches about investigating the relationship between solid particle size and final morphology of the droplet followed as a new

criteria were added to existing model. [13] The simulation of structural evolution of the particle was the main focus in this article.

Mezhericher et al. [14,15,16,1] also considered the particle morphology evolution during drying. The proposed theoretical model consisted of partial differential equations and appropriate boundary conditions for the temperature and the moisture distribution of the droplet. The model results validated and compared with experimental results available in literature [14]. For the mass transfer mechanism for internal vapor molecules a Stefan type diffusion was considered. Additionally thermal stresses present in the crust region were introduced and claimed to have important role in particle deformation [14,15]. Predictions and findings were carried further in the subsequent studies of the authors [16,1]. One of the most helpful papers was the one, which presented a novel mathematical model for the first stage of drying, as well as introducing and clarifying concepts like shell locking, shell strengthening, capillary forces at water interface etc [1]. The constant rate evaporation was similar to previous papers in the literature, nevertheless an elaborately investigated and well described receding process of evaporation interface was studied as well as other key components of the process such as theoretical maximum solid fraction, required shell strength in order to cease receding along with the water interface and the criteria for the final droplet morphology.

Liming et al. [17] proposed an experimental determination and mathematical model investigating both the effect of air temperature on droplet drying as well as the evolution of particle morphology. Proposed model includes a relatively simpler approach based on experimental observations than commonly studied models which in general consist of partial differential equations that have to be solved simultaneously. Experimental results for different air temperature values are compared with the results presented by Nesic and Vodnik [6] and discussed in detail.

Providing a significant basis for this study, concepts presented by Handscomb et al. [12] such as wet shell, dry crust, shell thickening, cease of receding etc. are also mentioned in upcoming sections. On the other hand, although only the first stage of evaporation was studied in Mezhericher et al. [1], the mentioned concepts have significant importance for morphological analysis and determining reasonable assumptions throughout the drying process. Besides, PDEs introduced in Dalmaz et al. [9] are constructing the main frame of this study, improved with above concepts coming into play as phase transition criteria and several boundary conditions. Unlike most of the previous studies in the literature, concepts such as the emergence of vacancy and its behavior dependent on the shell movement are taken into consideration. Furthermore, COMSOL simulation provides a distinct approach to the analysis of the proposed model.

CHAPTER 3

MODELING AND SIMULATION

3.1. Modeling of Drying Process

A mathematical model describing the drying kinetics of a single droplet with suspended solid particles is proposed. The model generally utilized main concepts presented in previous studies [9,12,1,6]. Both constant rate and falling rate of evaporation stages are modeled with partial differential equations and corresponding boundary conditions.

Initially the droplet is assumed to have certain amount of solid particles with relatively low volume fraction; hence, the liquid undergoes a free evaporation at the beginning of drying process. As the receding evaporation interface falls behind the solid particles, which just formed a stable shell that can withstand against the forces exerted by receding water molecules, second stage of drying begins. Initial conditions of the second stage are determined as the final conditions of the first stage, where a significantly different process is at hand. Evaporation of water continues from the receding interface of water molecules, whereas water molecules at the center of the droplet begins to move through the slurry region to the evaporation front after no solid particles remain in the slurry region, creating a vacancy at the center. Related mechanism of both stages and certain incident intervals are specified in detail in the subsequent sections.

3.1.1. Modeling of the First Stage

The very first structure of the droplet contains suspended solid particles in certain amount of water with relatively high initial water volume fraction (Fig 3.1). Heat is transferred to the droplet convectively by flowing air, further conducted to inner regions with conduction. Evaporation occurs at water surface, leading to a reduction in droplet size (Fig 3.2). Subsequent mechanisms are agglomeration of solid particles, locking, shell formation, shell thickening and cease of shell movement, as they were already mentioned in previous sections. First stage of drying involves the time interval until water interface falls behind the shell outer boundary.
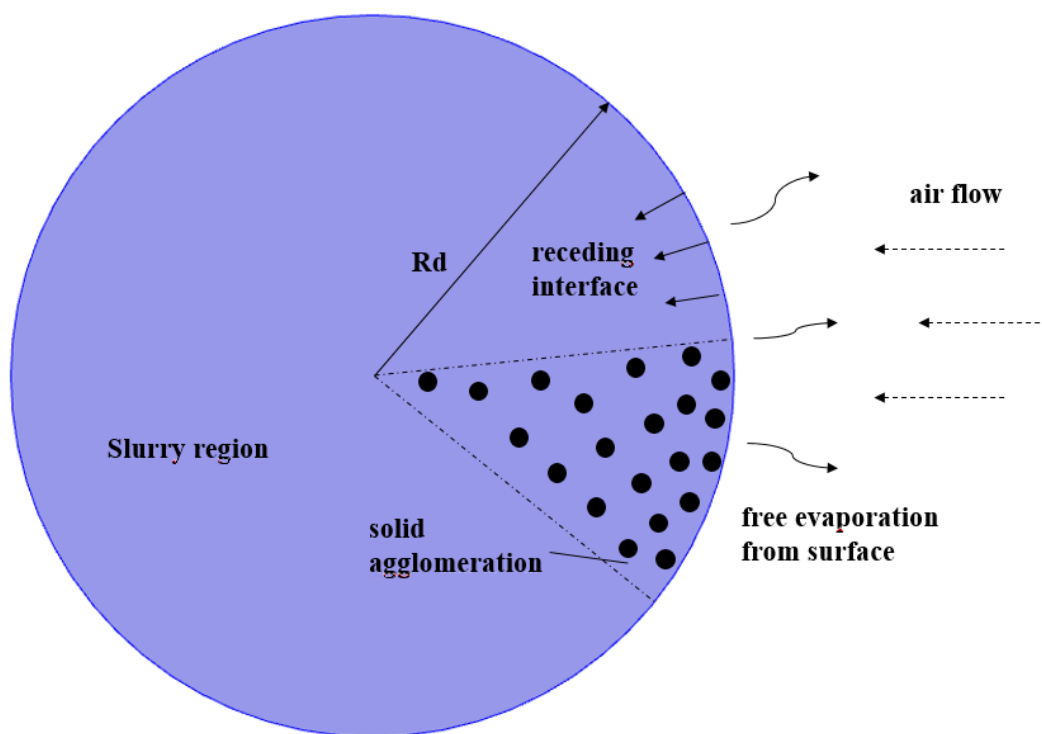
Figure 3.1. A nanosuspension droplet at initial drying stage

Throughout the first stage of drying, various assumptions are taken into account in order to simplify the calculations. These are,

1. Droplet is assumed to preserve its spherical shape at all times

2. Properties of water, air, solid (SiO_2) and water vapor are assumed constant at an average temperature

3. Nanosized solid particles are assumed to be at the same size in accordance with the continua approach

4. Heat transfer mechanisms are convection for the surface and conduction for inner regions of the particle

5. Temperature and concentration are considered to change only in radial direction
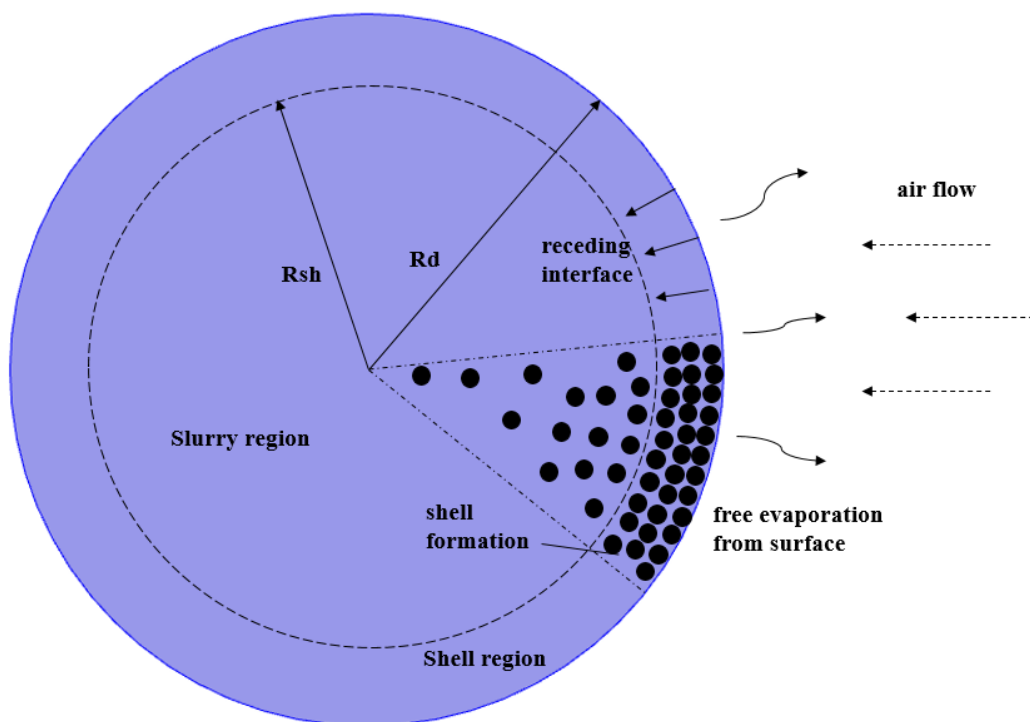
Figure 3.2. Formation of shell in the first stage

6. Gases present in the system are assumed as ideal

7. There is no chemical interaction between any of the materials

8. Flow direction of ambient air is assumed to disrupt neither the form nor the internal transfer kinetics of the droplet

9. Solid particles are initially distributed uniformly throughout the droplet, however uniformity is disrupted for $t > 0$

At first, the droplet is in slurry form, containing solid particles uniformly distributed within the droplet. Heat balance equations are required to describe both convective heat receive and conductive heat transfer through the inner region. Following differential equation is obtained as

For $0 \leq r \leq R_d, t > 0$

$$\frac{\partial T_{sl}}{\partial t}(\varphi_w \rho_w cp_w + \varphi_s \rho_s cp_s) = -\frac{1}{r^2}\frac{\partial}{\partial r}(r^2 q_{sl}) \qquad (3.1)$$

where letters R, T, φ, ρ, cp and q stand for radius, temperature, volume fraction, density, specific heat and heat conducted; whereas subscripts d, sl, w and s stand for droplet, slurry, water and solid, respectively.

Fourier's law of conduction states that,

$$q = k\frac{\partial T}{\partial r} \qquad (3.2)$$

Introducing into PDE

$$\frac{\partial T_{sl}}{\partial t}(\varphi_w \rho_w cp_w + \varphi_s \rho_s cp_s) = -\frac{1}{r^2}\frac{\partial}{\partial r}\left(r^2 k_{sl}\frac{\partial T_{sl}}{\partial r}\right) \tag{3.3}$$

where k stands for heat conductivity and defined as

$$k_{sl} = \varphi_w k_w + \varphi_s k_s \tag{3.4}$$

$$\varphi_s = 1 - \varphi_w \tag{3.5}$$

After some arrangements initial PDE takes its final form such as

$$\alpha_1 \frac{\partial T_{sl}}{\partial t} = \frac{\partial^2 T_{sl}}{\partial r^2} + \frac{2}{r}\frac{\partial T_{sl}}{\partial r} \tag{3.6}$$

where coefficient defined as α_1 is

$$\alpha_1 = \frac{(\varphi_w \rho_w cp_w + \varphi_s \rho_s cp_s)}{k_{sl}} \tag{3.7}$$

Corresponding initial and boundary conditions for heat balance PDE can be expressed such as,

Initial condition for $0 \leq r \leq R_d, t = 0$

$$T_{sl} = T_{initial} \tag{3.8}$$

Boundary condition for $r = 0, t > 0$

$$-k_{sl}\frac{\partial T_{sl}}{\partial r} = 0 \tag{3.9}$$

Boundary condition for $r = R_d, t > 0$

$$\lambda_w \rho_w \frac{dR_d}{dt} = h(T_{sl} - T_{air}) + k_w \frac{\partial T_{sl}}{\partial r} \tag{3.10}$$

where letters λ and h stand for latent heat of evaporation and convective heat transfer coefficient. After some arrangements, PDE for second boundary condition takes the form below

$$\frac{dR_d}{dt} = \alpha_2(T_{sl} - T_{air}) + \alpha_3 \frac{\partial T_{sl}}{\partial r} \tag{3.11}$$

where corresponding coefficients are defined as

$$\alpha_2 = \frac{h}{\lambda_w \rho_w} \tag{3.12}$$

$$\alpha_3 = \frac{k_w}{\lambda_w \rho_w} \tag{3.13}$$

In order to calculate heat transfer coefficient in equation 3.10, an empirical correlation is utilized, whose simpler version was first presented by Ranz and Marshall [2]. Convective heat transfer coefficient depends on various properties of both flowing fluid and drying particle. The compact form of convective heat transfer coefficient equation is given as

$$h = Nu \frac{k_a}{d_p} \qquad (3.14)$$

where Nu is Nusselt number, k and d represent heat conductivity and diameter and subscripts a and p stand for air and particle.

For a better understanding of how convective heat transfer coefficient is determined, open form of above equation should be described where equation of Nusselt number should be written first

$$Nu = 2 + 0.65(Re)^{0.5}(Pr)^{0.33} \qquad (3.15)$$

The definition of Nusselt number introduces two more empirical constants to be investigated, that are Reynolds and Prandtl number

$$Re = \frac{d_p v_a \rho_a}{\mu_a} \qquad (3.16)$$

$$Pr = \frac{cp_a \mu_a}{k_a} \qquad (3.17)$$

Terms that have not yet been introduced are velocity and viscosity, which are v and μ in above equations. Since all empirical constants are now presented, open form of convective heat transfer coefficient can be expressed by combining all these terms as given below

$$h = 2\frac{k_a}{d_p} + 0.65\left(\frac{v_a\rho_a}{d_p}\right)^{0.5} k_a{}^{0.67} cp_a{}^{0.33} \mu_a{}^{-0.17} \qquad (3.18)$$

Considering that the properties of flowing air are assumed as constant at an average temperature, the only variable that affects convective heat transfer coefficient is the particle diameter, which changes in the first stage only. Droplet shrinkage stops in the second stage since solid particles stabilize at a certain point and determine the final particle diameter. Thus, convective heat transfer coefficient is also assumed as constant throughout the second stage of drying process.

Second boundary condition of the heat balance PDE describes the motion of receding water interface. Besides, this motion can also be described with material balance approach, in which diffusion kinetics of evaporated water vapor are utilized. A material balance at water interface, i.e. for $r = R_d, t > 0$, yields

$$\rho_w \frac{dR_d}{dt} = -k_m M_w (c_{wv} - c_{air}) \qquad (3.19)$$

where k_m, M and c stand for mass transfer coefficient, molecular weight and moisture concentration, respectively. Subscript wv represents the water vapor concentration at the droplet surface while subscript air signifies the ambient air moisture.

In this case, concentration of water vapor at water interface changes constantly as evaporation occurs from the surface. Since vapor concentration depends only on temperature at water interface, equation for solving instantaneous vapor concentration can be expressed as

for $r = R_d, t > 0$

$$c_{wv} = \frac{(P_{vap})_{T_{sl}}}{R_g \times T_{sl}} \qquad (3.20)$$

where P_{vap} and R_g represent vapor pressure and gas constant, respectively. Vapor pressure of water vapor for corresponding temperature value can be calculated either by Antoine equation [18] as well as by other formulations, which are preferred to utilize in the simulation and will be introduced in following chapters.

Material balance PDE takes the following form after a slight arrangement

$$\frac{dR_d}{dt} = \alpha_4(c_{wv} - c_{air}) \qquad (3.21)$$

where the coefficient α_4 is defined as

$$\alpha_4 = \frac{-k_m M_w}{\rho_w} \qquad (3.22)$$

Initial condition for $r = R_d, t = 0$

$$R_d = R_{initial} \qquad (3.23)$$

Another coefficient coming into play with the introduction of equation 3.19 is mass transfer coefficient, which is also calculated with various empirical coefficients similar to convective heat transfer coefficient. The compact form of mass transfer coefficient is given as

$$k_m = Sh\frac{D_{wv}}{d_p} \qquad (3.24)$$

where Sh is Sherwood number. Diffusivity on the other hand is represented by D_{wv} and it describes the diffusivity of water vapor in air. Sherwood number is determined with various empirical constants such as Reynolds number, which is already introduced in equation 3.16 and Schmidt number given below

$$Sh = 2 + 0.65(Re)^{0.5}(Sc)^{0.33} \qquad (3.25)$$

$$Sc = \frac{\mu_a}{\rho_a D_{wv}} \qquad (3.26)$$

After substitutions of required terms into the equation 3.24, open form of mass transfer coefficient is obtained as

$$k_m = 2\frac{D_{wv}}{d_p} + 0.65\left(\frac{v_a}{d_p}\right)^{0.5}\left(\frac{\rho_a}{\mu_a}\right)^{0.17}D_{wv}^{\;0.67} \qquad (3.27)$$

Similar to convective heat transfer coefficient equation, only variable is particle diameter also for mass transfer coefficient equation, considering that air properties remain constant. This assumption again leads to a constant mass transfer coefficient in the second stage of drying, since diffusivity of water vapor is also assumed to remain constant just like droplet diameter.

First stage ends when the shell is thick enough to withstand the capillary forces exerted by receding water molecules at the evaporation interface. This criterion depends on various parameters such as solid material, solid volume fraction, thickness of shell etc., which determine the strength of the shell. However, this subject is out of the scope of this study.

Model equations involved in the first stage of drying process are presented step by step in this section. There are considerable numbers of constants in first stage model equations, whose values for corresponding temperature values are listed in Appendix-A section.

3.1.2. Modeling of the Second Stage

The very first structure of the droplet in the second stage can be described with three sections, namely slurry region, (wet) shell region and (dry) crust region, from inside out as shown in Figure 3.3. The moment when water interface falls under the outermost line of the solid particles can be considered as the initial time of the second stage.

The region between the outermost solid particles and water interface is called dry crust, in which only closely packed solid particles and evaporated water vapor, which are diffusing through pores, and air are present. Solid particles in both crust and shell regions are assumed to be packed with a maximum possible fraction, similar to the assumption in previous studies [1]. The region between water interface and inner boundary of the wet shell is called as shell region, where receding continues to occur through the pores of solid particles. As water interface falls back, more and more solid particles join the crust region automatically. Whereas droplet size, i.e. R_d, reduces constantly in the first stage of drying, size reduction ceases in the second stage where solid particles form a stable shell at the outermost part of the droplet.
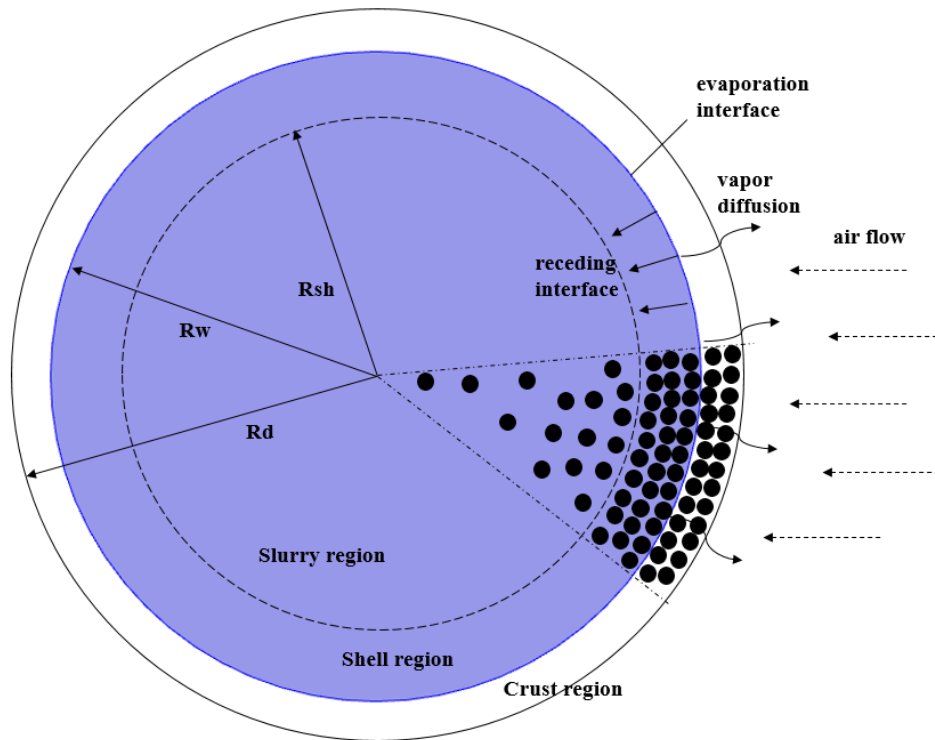
Figure 3.3. Structural overview of the droplet at second drying stage

Adherence of particles from the slurry region to the shell causes a continuous shell thickening, until complete consumption of solid particles in the innermost region (Fig 3.4). This incident can be considered as one of the most important mechanisms in this stage because it continuously changes the water/solid volume fraction in the slurry region. Main reason for such fractional change is that the porosity in shell and slurry regions are different from each other, whereas adherence of solid particles has to be at a fraction similar to the shell. This is actually one of the essential assumptions directly affecting the equations in the model. To be more specific, volume fraction of water in slurry region is greater than the one in shell region and the assumption is that, water molecules in the inner region have the tendency to compensate the water, which is lost by evaporation. Therefore, for the water inside a driving force towards the evaporation interface arises. This leads to diffusion of both solid and water molecules

outwards, also resulting in shell thickening as mentioned earlier. However shell region always retains its porosity, which is significantly smaller than porosity, i.e. water volume fraction, in slurry region, thus more solid particles diffuse to the shell-slurry interphase in comparison to water molecules. Consequently, volume fraction of water in slurry constantly increases until all solid particles join the shell. This point also marks the end of shell thickening and shell inner boundary, i.e. R_{sh}, remains constant from now on.
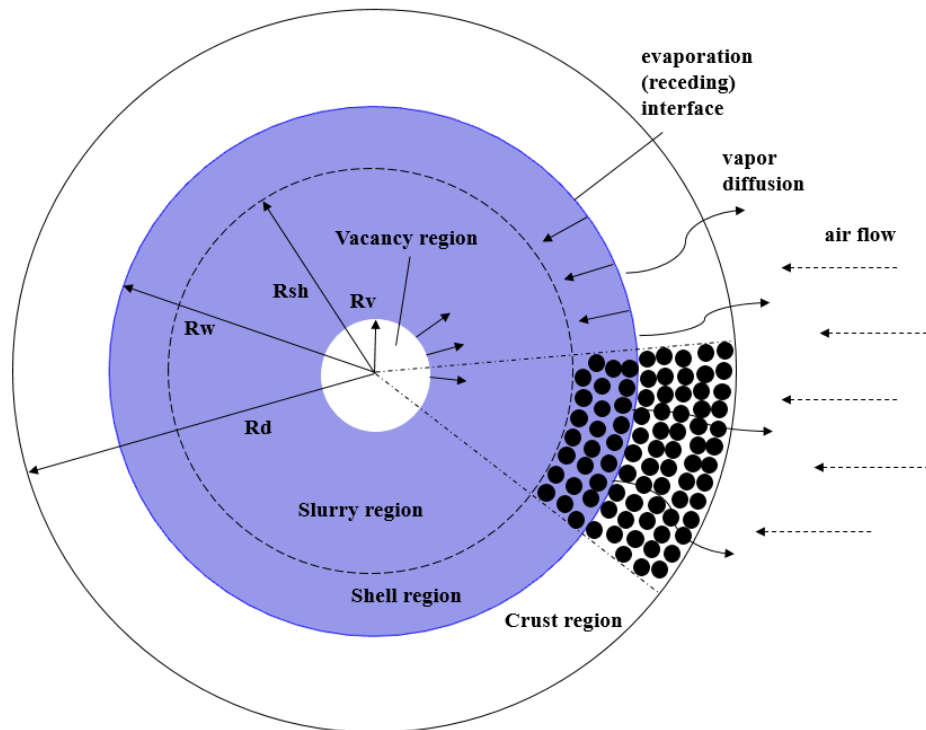
Figure 3.4. Depletion of solids in slurry and emergence of vacancy

Another important mechanism in this stage is the emergence of a vacancy at the center of the droplet (Fig 3.4). The driving force to compensate the lost water by evaporation still exists even if there is no solid particles remaining in slurry region. Therefore, a

very small hollow vacancy arises at the center of the droplet, as water molecules inside migrate to the evaporation front. On the other hand receding of water interface continues, hence there are two interfaces, which move towards each other in the late stages of the second stage of drying. When these two interfaces, namely vacancy interface R_{vc} and water interface R_w coincide with each other, no water is left in the particle that is now nothing but a hollow solid dry crust.
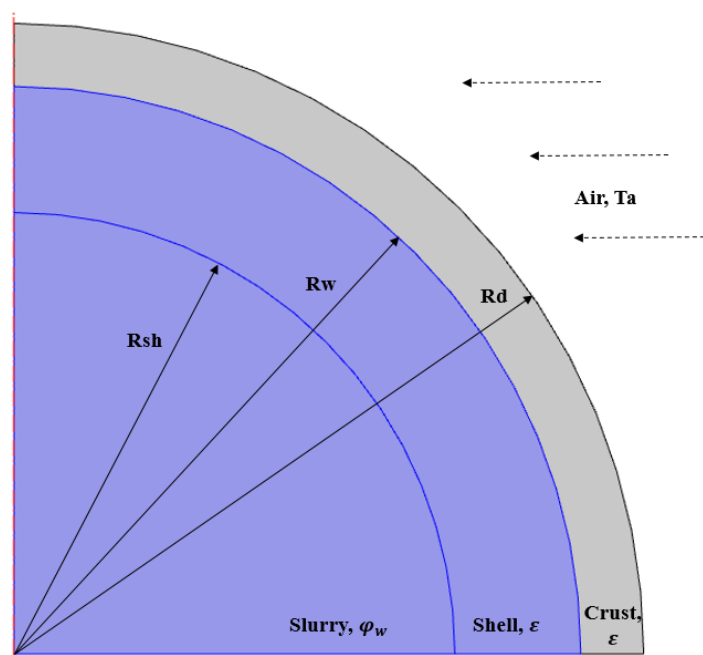
Figure 3.5. Boundaries at early second stage

General assumptions for second stage of drying are listed below,

1. Droplet is assumed to preserve its spherical shape and droplet size is constant throughout the second stage

2. Properties of water, air, solid (SiO_2) and water vapor are assumed constant at an average temperature

24

3. Heat transfer mechanisms are convection for the outer crust interface and conduction for inner regions of the particle

4. Temperature and concentration change only in radial direction

5. Movement of the interfaces occur only in radial direction

6. There is no chemical interaction between any of the materials

7. Gases present in the system are assumed as ideal

8. Flow direction of ambient air is assumed to disrupt neither the form nor the internal kinetics of the droplet

9. Initial solid volume fraction in slurry region is always smaller than the one in shell and crust regions

10. The final particle morphology is always hollow solid particle because of previous assumption

11. Solid particles are non-uniformly distributed throughout the slurry region, in a manner that the solid volume fraction is higher at the points closer to the shell and at the very interface ($r \cong R_{sh}$) equal to the shell solid volume fraction

12. Vacancy is assumed to contain negligible amount water vapor and no evaporation occurs at the vacancy boundary during the drying process

13. Air-vapor mixture is present in crust region, where respective properties such as conductivity etc. are estimated with averaging at a constant ratio

14. Concentration of water in shell region is constant as opposed to the slurry region until all solid particles are joined to shell region. After complete depletion of solids, volume fraction of water in slurry region is equated to 1

15. Vacancy emerges at the very center of the droplet just after the solid particles in slurry region are depleted.

16. Diffusivity of water molecules is assumed as constant in both slurry and shell regions, even though the porosities are not equal and vary in some locations

Since there are several regions and boundaries in this stage of drying as shown in Figure 3.5, mass and energy equations are described for each, in order to have a continuous description of conservation laws throughout the droplet. First region to analyze is the outer most region of the droplet i.e. crust region. Heat balance for dry crust is obtained such as

For $R_w \leq r \leq R_d, t > 0$

$$\frac{\partial T_{cr}}{\partial t} [\varepsilon \rho_v cp_v + (1 - \varepsilon)\rho_s cp_s] = \frac{-1}{r^2} \frac{\partial}{\partial r} (r^2 q_{cr}) - \frac{1}{r^2} \frac{\partial}{\partial r} (r^2 T_{cr} cp_v J_{cr}) \tag{3.28}$$

where flux term which is indicated by J is given as

$$J_{cr} = -D_{cr} M_{wv} \frac{\partial c_{wv}}{\partial r} \tag{3.29}$$

and heat conducted through crust

$$q_{cr} = -k_{cr} \frac{\partial T_{cr}}{\partial r} \tag{3.30}$$

It is noteworthy that air is assumed to be present in crust region with water vapor, its effects on physical parameters are also taken into account, but it will not be mentioned separately and the gaseous mixture in crust region will be called simply as water vapor.

Diffusivity of water vapor in the crust region is indicated by D_{cr} and defined as below[19], meaning that water vapor diffusivity is smaller than its actual value in a porous matrix.

$$D_{cr} = \frac{2\varepsilon D_{wv}}{3 - \varepsilon} \tag{3.31}$$

Thermal conductivity of the crust region is determined by simple volume averaging of conductivities of present materials in that region. Hence,

$$k_{cr} = \varepsilon k_v + (1 - \varepsilon)k_s \tag{3.32}$$

After necessary arrangements, the partial differential equation 3.28 takes the intermediate form such as

$$\beta_1 \frac{\partial T_{cr}}{\partial t} = \frac{-1}{r^2}\frac{\partial}{\partial r}(r^2 q_{cr}) - \frac{\beta_2}{r^2}\frac{\partial}{\partial r}\left(r^2 T_{cr}\frac{\partial c_{wv}}{\partial r}\right) \tag{3.33}$$

where coefficients β_1 and β_2 are defined as

$$\beta_1 = \frac{\varepsilon \rho_v c p_v + (1 - \varepsilon)\rho_s c p_s}{k_{cr}} \tag{3.34}$$

$$\beta_2 = \frac{D_{cr}M_w c p_v}{k_{cr}} \tag{3.35}$$

Final arrangement includes collecting terms with similar differential dependencies

$$\beta_1 \frac{\partial T_{cr}}{\partial t} = \frac{\partial^2 T_{cr}}{\partial r^2} + \left(\frac{2}{r} + \beta_2 \frac{\partial c_{wv}}{\partial r}\right)\frac{\partial T_{cr}}{\partial r} + \left(\frac{2\beta_2}{r}\frac{\partial c_{wv}}{\partial r} + \beta_2 \frac{\partial^2 c_{wv}}{\partial r^2}\right)T_{cr} \qquad (3.36)$$

Equation 3.36 is the main partial differential equation for heat balance at crust region in the second stage of drying process. In order to solve it, two boundary and one initial conditions are required, specifying the situation at adjacent boundaries and initial case.

Initial condition for $R_w \leq r \leq R_d, t = 0$

$$T_{cr} = T_{1,final} \qquad (3.37)$$

where $T_{1,final}$ stands for the final temperature of the first stage of drying in corresponding region.

Boundary condition for $r = R_d, t > 0$

$$-k_{cr}\frac{\partial T_{cr}}{\partial r} = h(T_{cr} - T_{air}) \qquad (3.38)$$

Boundary condition for $r = R_w, t > 0$

$$\varepsilon \rho_w \lambda_w \frac{dR_w}{dt} = -k_{cr}\frac{\partial T_{cr}}{\partial r} + k_{sh}\frac{\partial T_{sh}}{\partial r} \qquad (3.39)$$

where subscript sh indicates shell.

Boundary conditions for the equation 3.36 are actually interpreted by a simple heat balance from convective air to the crust region for crust boundary and heat balance

28

involving conductive heat transfer from crust to shell and also heat loss by evaporation at water interface, R_w.

Given boundary conditions can also be written in their compact forms such as

$$\frac{\partial T_{cr}}{\partial r} = \beta_3 (T_{cr} - T_{air}) \tag{3.40}$$

where

$$\beta_3 = -\frac{h}{k_{cr}} \tag{3.41}$$

and

$$\frac{dR_w}{dt} = \beta_4 \frac{\partial T_{cr}}{\partial r} + \beta_5 \frac{\partial T_{sh}}{\partial r} \tag{3.42}$$

where

$$\beta_4 = \frac{-k_{cr}}{\varepsilon \rho_w \lambda_w} \tag{3.43}$$

$$\beta_5 = \frac{k_{sh}}{\varepsilon \rho_w \lambda_w} \tag{3.44}$$

Description of the mass transfer operations taking place in crust region is obtained by taking a differential volume element and analyzing changes in water vapor concentration with respect to both time and position

$$\frac{\partial}{\partial t} (\varepsilon M_{wv} c_{wv}) = \frac{-1}{r^2} \frac{\partial}{\partial r} (r^2 J_{cr}) \tag{3.45}$$

Since flux term is already given in equation 3.29, intermediate steps of arrangement are skipped and final form of above partial differential equation is expressed as

$$\beta_6 \frac{\partial c_{wv}}{\partial t} = \frac{\partial^2 c_{wv}}{\partial r^2} + \frac{2}{r} \frac{\partial c_{wv}}{\partial r} \qquad (3.46)$$

where

$$\beta_6 = \frac{\varepsilon}{D_{cr}} \qquad (3.47)$$

Similar to heat balance equation for crust region, mass balance equation given in 3.46 also requires two boundary and one initial conditions.

Initial condition for $R_w \leq r \leq R_d, t = 0$

$$c_{wv} = \frac{(P_{vap})_{T_{cr}}}{R \times T_{cr}} \qquad (3.48)$$

where T_{cr} is initial temperature of the crust region, that can also be expressed with $T_{1,final}$. Initial moment of second stage provides a very tiny distance between R$_w$ and R$_d$, thus crust region may be assumed as filled with water vapor at its saturation concentration initially.

Boundary condition for $r = R_d, t > 0$

$$-D_{cr} \frac{\partial c_{wv}}{\partial r} = k_m(c_{wv} - c_{air}) \qquad (3.49)$$

that can also be written in a more compact form such as

$$\frac{\partial c_{wv}}{\partial r} = \beta_7(c_{wv} - c_{air}) \qquad (3.50)$$

where

$$\beta_7 = -\frac{k_m}{D_{cr}} \tag{3.51}$$

Boundary condition for $r = R_w, t > 0$

$$c_{wv} = \frac{(P_{vap})_{T_{cr}}}{R \times T_{cr}} \tag{3.52}$$

It can be easily realized that initial condition and boundary condition at water interface for mass transfer in crust region is the same. However, since the temperature of water interface constantly changes in time, concentration of water vapor changes as well.

Most of the important incidents are taking place in crust region and at its boundaries. Nevertheless, it would be also useful to take a look at inner regions, i.e. shell and slurry before investigation of boundary movements. Since some of the boundary conditions are shared with adjacent regions, they are not specifically stated. Other than that, for inner regions heat balances are given as an equation set derived from conservation laws, whereas mass balance operations are utilized for describing motion interfaces instead of writing them for the whole region since the significance of boundary movements is considerably substantial.

Heat balance in a differential volume element in shell region yields similar expression as equation 3.1

$$\frac{\partial T_{sh}}{\partial t}(\varepsilon\rho_w cp_w + (1-\varepsilon)\rho_s cp_s) = -\frac{1}{r^2}\frac{\partial}{\partial r}(r^2 q_{sh}) \tag{3.53}$$

where heat conduction in shell is given by

$$q_{sh} = k_{sh}\frac{\partial T_{sh}}{\partial r} \tag{3.54}$$

and thermal conductivity of shell region is determined by volume average of water and solid conductivities, such as

$$k_{sh} = \varepsilon k_w + (1 - \varepsilon)k_s \tag{3.55}$$

After necessary substitutions and arrangements, equation 3.53 takes the form

$$\gamma_1\frac{\partial T_{sh}}{\partial t} = \frac{\partial^2 T_{sh}}{\partial r^2} + \frac{2}{r}\frac{\partial T_{sh}}{\partial r} \tag{3.56}$$

where

$$\gamma_1 = \frac{[\varepsilon\rho_w cp_w + (1 - \varepsilon)\rho_s cp_s]}{k_{sh}} \tag{3.57}$$

Similar to previous PDEs, two boundary and one initial conditions are required in order to solve equation 3.56.

Initial condition for $R_{sh} \leq r \leq R_w, t = 0$

$$T_{sh} = T_{1,final} \tag{3.58}$$

where $T_{1,final}$ stands for the final temperature of the first stage of drying in corresponding region.

Boundary condition for $r = R_w, t > 0$ is the same as equation 3.39 whereas boundary condition for $r = R_{sh}, t > 0$ can be expressed as

$$k_{sl}\frac{\partial T_{sl}}{\partial r} = k_{sh}\frac{\partial T_{sh}}{\partial r} \qquad (3.59)$$

where

$$k_{sl} = \varphi_w k_w + \varphi_s k_s \qquad (3.60)$$

The shell region is assumed to have constant porosity filled with water. Similar to crust region, solid particles in shell are also packed with the same fraction. Thus, concentration of water molecules in that region can be written as

For $R_{sh} \leq r \leq R_w, t \geq 0$

$$c_w = \varepsilon\frac{\rho_w}{M_w} \qquad (3.61)$$

Motion of water interface can be tracked with a mass balance at water boundary, in which evaporated water amount is equated to mass of diffusing water vapor at the same interface, such as

$$\varepsilon\rho_w\frac{dR_w}{dt} = M_w D_{cr}\frac{\partial c_{wv}}{\partial r} \qquad (3.62)$$

Above equation can be reduced in a more compact form as below

$$\frac{dR_w}{dt} = \gamma_2\frac{\partial c_{wv}}{\partial r} \qquad (3.63)$$

where

$$\gamma_2 = \frac{D_{cr}M_w}{\varepsilon\rho_w} \qquad (3.64)$$

33

Although another equation for motion of water interface can also be obtained by leaving differential term alone in equation 3.39 at the left hand side, equation 3.63 is more appropriate to use since it is derived from a mass balance at corresponding boundary.

Another region that should be investigated is slurry region, where equations get complicated at a fair amount. One of the most important assumptions taken into consideration is that volume fraction of water throughout the slurry region is not constant until it reaches to one, i.e. when all solid particles adhere to inner shell boundary. It is also noteworthy that initial value of φ_w is an important parameter for simulation part, which affects mainly the duration of certain incidents throughout the drying process. Additionally, as it is already mentioned in previous sections, distribution of solid particles in slurry region is non-uniform in the second stage, where particles are much more condensed at regions close to shell inner boundary in comparison to the regions close to the center of the droplet or vacancy boundary after certain time. The main reason for such an agglomeration event to occur is that evaporation process and receding of water interface takes place quite fast, so that particles inside fail to arrange themselves again uniformly throughout the region they belong to. On the other hand, the assumption that as solid particles adhere to shell inner boundary, they become a part of the shell with constant porosity of ε, is another logical reason to consider the non-uniformity in slurry region. These considerations enable the volume fraction of water in slurry to take a value between initial value of $\varphi_{w,i}$ and 1 for $t > 0$.

Heat balance in a differential volume element in slurry region gives

$$\frac{\partial T_{sl}}{\partial t}(\varphi_w \rho_w cp_w + (1 - \varphi_w)\rho_s cp_s) = -\frac{1}{r^2}\frac{\partial}{\partial r}(r^2 q_{sl}) \qquad (3.65)$$

where

$$q_{sh} = k_{sl} \frac{\partial T_{sl}}{\partial r} \tag{3.66}$$

and thermal conductivity of slurry region is determined by volume average of water and solid conductivities, such as

$$k_{sl} = \varphi_w k_w + (1 - \varphi_w)k_s \tag{3.67}$$

After some arrangements equation 3.65 becomes as given below

$$\gamma_2 \frac{\partial T_{sl}}{\partial t} = \frac{\partial^2 T_{sl}}{\partial r^2} + \frac{2}{r} \frac{\partial T_{sl}}{\partial r} \tag{3.68}$$

where

$$\gamma_2 = \frac{[\varphi_w \rho_w c p_w + (1 - \varphi_w)\rho_s c p_s]}{k_{sl}} \tag{3.69}$$

Initial condition for $0 \leq r \leq R_w, t = 0$

$$T_{sl} = T_{1,final} \tag{3.70}$$

where $T_{1,final}$ stands for the final temperature of the first stage of drying in corresponding region.
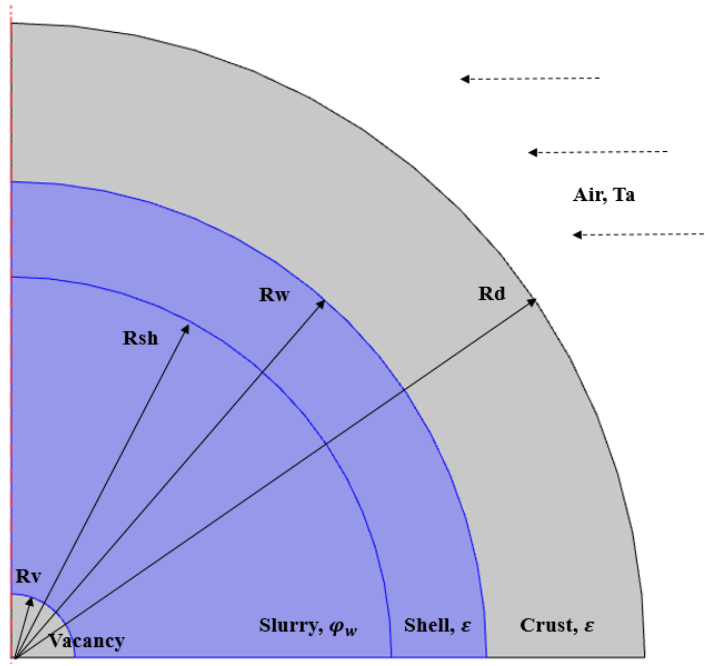
Figure 3.6. Boundaries after vacancy emergence in second stage

Boundary condition for $r = R_{sh}, t > 0$ is the same as equation 3.59 and boundary condition for $r = 0, 0 < t < t_{vc}$ is the same as equation 3.9. However, as stated in boundary condition specifications equation 3.9 is only valid until a vacancy emerges at the center of the droplet. After that instant, which is described with t_{vc}, inner boundary of slurry region or in other words radius of vacant region is described as R_{vc} i.e. vacancy boundary (Fig 3.6). Thus,

Boundary condition for $r = R_{vc}, t > t_{vc}$

$$T_{sl} = T_{vc} \tag{3.71}$$

Further assumptions for simplification are considered at this point. Since heat and mass kinetics happening inside of vacant region is not included in the scope of this

study, temperature and concentration of water at vacancy boundary are directly equated to the corresponding dependent variable in slurry region. Equation 3.71 describes that temperature of vacancy boundary is equal to temperature of adjacent points in slurry region. On the other hand, concentration of water can be written as

For $0 \leq r \leq R_w, 0 \leq t \leq t_{vc}$ and for $R_{vc} \leq r \leq R_w, t \geq t_{vc}$

$$c_w = \varphi_w \frac{\rho_w}{M_w} \tag{3.72}$$

where

$$\varphi_w = \frac{R_{sh,i}{}^3 \varphi_{w,i} - \left(R_{sh,i}{}^3 - R_{sh}{}^3\right)\varepsilon}{R_{sh}{}^3} \tag{3.73}$$

where subscript i describes initial values. Above equation can simply be explained as such, where properties of all terms belong to slurry region

$$\varphi_w = \frac{initial\ water\ amount - migrated\ water}{volume\ of\ water} \tag{3.74}$$

Since it is assumed that solid particles close to shell inner boundary have higher local fraction similar to the ones in shell region, water molecules migrating from slurry to shell are represented as a loss with ε in equation 3.73. Only variable causing φ_w to change is R_{sh}, whose movement means adherence of solid particles, as mentioned before. Therefore, movement of inner shell boundary ceases automatically when no solid particle remain in slurry region, i.e. when volume fraction of water in that region reaches to one. This instant, also called as t_{vc} is when vacancy emerges at the center of the droplet, and this time another boundary movement begins outwards from center that is represented by R_{vc}.

The motion of inner shell boundary is obtained with guidance of an illustration demonstrated in Figure 3.7. The assumption is that receding of the water interface as evaporation takes place causes the wet region, i.e. shell and slurry, to shrink and leads to agglomeration and adherence of solid particles to shell. Since R_{sh} is defined as shell inner boundary, as R_w moves inwards so does R_{sh}. Additionally, recalling that the porosities of the boundaries just at their corresponding inner sides are equal to each other, this dependent motion can be described with the ratio of squares of boundary radii.
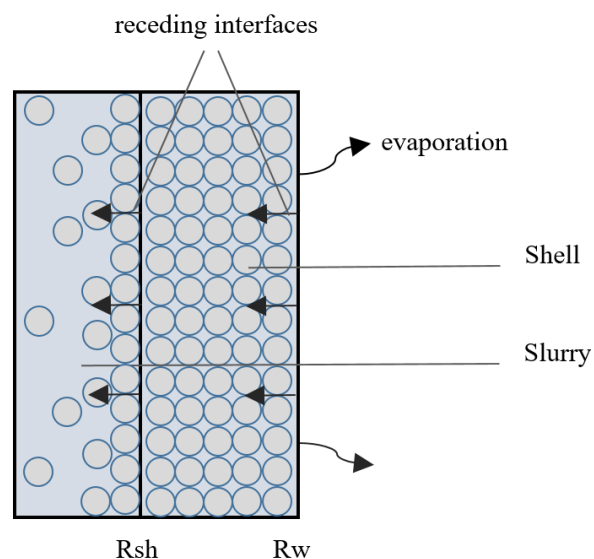
Figure 3.7. Motion of shell interfaces

Corresponding derivation shows that

$$4\pi R_w{}^2 dR_w = 4\pi R_{sh}{}^2 dR_{sh} \qquad (3.75)$$

where volume of shrinkage is equated for both interfaces and obtained through product of an infinitesimal change in interfaces with corresponding surface area. Introducing time derivative and arranging the equation yields

$$\frac{dR_{sh}}{dt} = \frac{R_w{}^2}{R_{sh}{}^2} \frac{dR_w}{dt} \tag{3.76}$$

Equation 3.76 gives the motion of inner shell boundary or in other words, boundary of slurry region until water volume fraction in that region becomes one.

Afterwards emergence of a very small vacancy at the center is assumed, which grows in time and is again dependent of motion of the water interface. The idea behind the growth of vacancy is that water molecules in slurry have a tendency to compensate the lost water from the evaporation front, so that they migrate towards the evaporation front leaving a vacant region behind, which is assumed to contain water vapor. According to that assumption, both moving interfaces are supposed to meet at a surface somewhere in shell region, considering that water molecules tend to adhere to surface of solid particles instead of completely falling behind shell inner boundary.

The motion of vacancy boundary is estimated according to the assumption stated above. As water molecules diffuse towards the evaporation interface, they pass through the shell inner boundary with an amount that could compensate lost water by evaporation. Hence, motion of that boundary is obtained as

$$\frac{dR_{vc}}{dt} = \varepsilon \frac{R_w{}^2}{R_v{}^2} \frac{dR_w}{dt} \tag{3.77}$$

Simultaneously solving all these equations yields heat and concentration profiles for all times. Drying process of the droplet continues until all water molecules are evaporated, i.e. when vacancy and water interfaces coincide. As mentioned before, shell structure reaches its final form in early stages of the second stage of drying and fundamental parameter that affects shell formation process in this study is volume fraction of particles at the beginning of second stage.

The simulation part is prepared with COMSOL, in which various modules are utilized. Each module with its corresponding characteristics will be analyzed to clarify how presented model is adapted to the program.

3.2. Simulation of the Model

Drying process of a single droplet containing suspended solid particles is simulated with COMSOL Multiphysics, which is a powerful computational program used to model and solve scientific and engineering problems. It offers many features that enable almost any physical structure to be constructed and related mechanisms to be studied.

Simulation of the model is presented in sections, categorized by their corresponding physics. In order to simulate the drying process a couple of physics modules are required, which are basically transport module, heat transfer module and deformed geometry module. Additionally motion of the boundaries are estimated by utilization of boundary ordinary differential equations module.

3.2.1. General Characteristics and Structure

The model is demonstrated in a 2-D axisymmetric component since the structure of the droplet is assumed perfectly spherical. It is sufficient to demonstrate all physical operations in one-half cross section of the droplet because of axisymmetry.

Initially parameters and variables of the model are defined. Numerical values of parameters are presented in detail in the Appendix section. Content of parameters includes general structural properties such as dimensions of droplet layers, ambient temperature, crust properties etc. and also properties of water, solid, air and vapor individually. On the other hand, variables involve important properties, which are to be tracked during the drying process, such as volume fraction of water in slurry region, evaporated water vapor concentration just above the water interface and various other coefficients.

The constructed geometry must meet necessary requirements in order to solve the problem with one single study step, for the sake of simplicity. Therefore several assumptions are taken into consideration, otherwise the whole drying process must have been compiled in two or three consecutive study steps. For instance, even in initial case there is a very small area structurally defined as a vacancy present at the center of the droplet, even though vacancy emerges after water volume fraction in the slurry region increases to one. Besides, in order to avoid structural constraints while executing receding motion of water interface and expanding motion of vacancy boundary, shell inner boundary is not constructed as a structural interface in geometry module, however it is mathematically calculated for every time step and tracked for the whole drying process. The reason for that is actually complications, which are caused by inner shell boundary layer, as other boundaries are slowly getting closer.

Advantages provided by ignoring inner shell boundary as a structure can be named in a simple way as having only one domain describing watery region, simplification of deformed geometry operations and getting one-step away from convergence issues. For the disadvantages the lack of structural tracking of R_{sh} and distinguishing slurry and shell region from each other by two modules in order to specify their corresponding porosities individually are notable emerging issues. This is overcame by a volume averaging operation for the mentioned regions that will be explained in transport mechanism section. A general picture of the initial structure of the droplet is demonstrated in Figure 3.8. In order to use in the next sections, domains are presented as numbered in the figure.
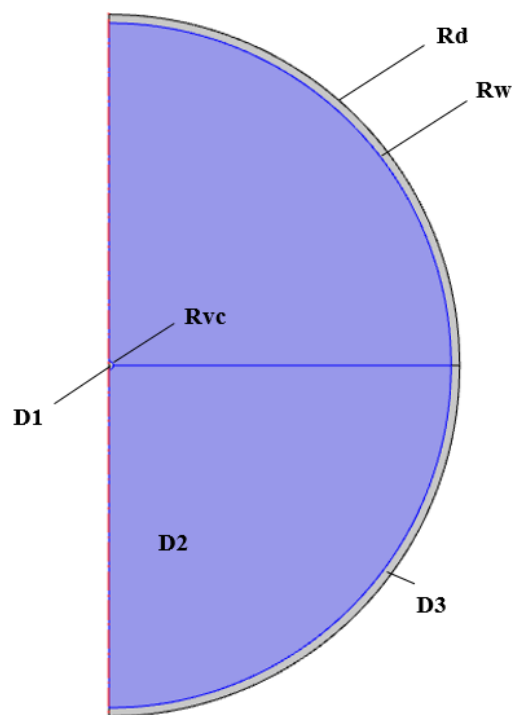
Figure 3.8. Initial structure of droplet domains in second stage

As can be seen in figure, simulation of the second stage of the drying process is not described for the moment just when water interface recedes behind solid particle. Instead, a very small distance between R_d and R_w is introduced initially in order not to tighten domain 3 too much so that it does not lead to requirement of very fine meshing.

The materials module available in the simulation program was not used since all properties of the materials are introduced into the simulation manually.

3.2.2. Transport Mechanism

Transport of water and water vapor is simulated with transport of diluted species module. The area between R_{vc} and R_w, i.e. D2, is defined as filled with water, whereas the area between R_w and R_d, i.e. D3, is defined as containing air-water vapor mixture, simply called as water vapor for the sake of simplicity.

Inherently these domains do not contain single material since initial structure involves solid particles throughout the whole droplet, thus the porosities must be described in relevant interfaces. Therefore, mass transfer in porous media option is enabled in transport mechanism interface. As a default interface, initial values for chosen domain must be clarified. Since domain 2 includes both slurry and shell region, an equation is obtained describing the water volume fraction for both regions as an average. At first, just for recalling the concentration equations for shell and slurry regions,

For $R_{sh} \leq r \leq R_w, t \geq 0$

$$c_w = \varepsilon \frac{\rho_w}{M_w} \tag{3.61}$$

For $R_{vc} \leq r \leq R_w, t \geq 0$

$$c_w = \varphi_w \frac{\rho_w}{M_w} \tag{3.72}$$

The spatial condition for equation 3.72 is updated because R_{vc} is already defined in the simulation at the initial time. Additionally the definition for water volume fraction given in equation 3.73 is also updated according to existence of R_{vc} such as,

$$\varphi_w = \frac{\left(R_{sh,i}{}^3 - R_{vc,i}{}^3\right)\varphi_{w,i} - \left(R_{sh,i}{}^3 - R_{sh}{}^3\right)\varepsilon}{\left(R_{sh}{}^3 - R_{vc}{}^3\right)} \tag{3.78}$$

A volume averaging for estimation of water concentration in D2 is determined by combining above equations with their corresponding volumetric fractions. Thus

$$c_{w,i} = \left(\frac{V_{sl,i}}{V_{liq,i}}\varphi_{w,i} + \frac{V_{sh,i}}{V_{liq,i}}\varepsilon\right)\frac{\rho_w}{M_w} \tag{3.79}$$

where V stands for volume and subscripts liq and i describe liquid and initial, respectively. Volumes introduced in above equation can be expressed such as

$$V_{liq,i} = R_{w,i}{}^3 - R_{vc,i}{}^3 \tag{3.80}$$

$$V_{sl,i} = R_{sh,i}{}^3 - R_{vc,i}{}^3 \tag{3.81}$$

$$V_{sh,i} = R_{w,i}{}^3 - R_{sh,i}{}^3 \tag{3.82}$$

44

As mentioned before, R_{sh} is not present in the simulation as a structural boundary; however, the value of R_{sh} is constantly calculated by a boundary ODE interface. Thus, R_{sh} is mathematically available in the simulation for all times.

Equation 3.79 is for the initial condition of D2 in transport module. However, water concentration changes with time and c_w must be determined by porous media transport properties interface for all times and position. Since the dependent variable of this module is the concentration of water, it will be automatically calculated in case the porosity of D2 is defined as a variable dependent of aforementioned volumetric fractions. Average porosity of shell and slurry regions, i.e. D2, can be described as below

$$porosity = \frac{V_{sl}}{V_{liq}} \varphi_w + \frac{V_{sh}}{V_{liq}} \varepsilon \qquad (3.83)$$

where

$$V_{liq} = R_w{}^3 - R_{vc}{}^3 \qquad (3.84)$$

$$V_{sl} = R_{sh}{}^3 - R_{vc}{}^3 \qquad (3.85)$$

$$V_{sh} = R_w{}^3 - R_{sh}{}^3 \qquad (3.86)$$

In equation 3.83, all terms are variables except ε. Because of constant change of water volume fraction in slurry, R_{sh} up to and R_{vc} from a certain time and R_w for all times, the concentration of water in D2 also changes continuously.

Other than initial values and porous media properties, diffusivity of water in that region and boundary conditions for D2 must be introduced. A significant assumption comes into play at this point, where the diffusivity of liquid water is assumed as constant regardless of the porosity of the medium, at a certain value indicated with D_w. Additionally; the concentrations at adjacent boundaries are equated to dependent variable concentration. Material removal by evaporation will be described with deformed geometry module, therefore there is no need to introduce any flux outwards from water interface in this module.

In order to simulate the transport mechanism of vapor in D3, again mass transfer in porous media options is enabled in mass transfer interface, where dependent variable is concentration of water vapor. The initial value of water vapor concentration present in D3 is assumed as basically the saturation concentration of vapor at initial temperature. The equation for saturation concentration of water vapor at any temperature is given in equations in heat transfer manual of the simulation program [20] such as

$$c_{wv,sat} = \frac{610.7 \times 10^{\left(7.5 \times \frac{T-273.15}{T-35.85}\right)}}{R \times T} \tag{3.87}$$

This equation can be used for describing both initial condition and general condition as long as T is defined as the temperature of region D3.

The porosity in dry crust is constant for all times and indicated with ε. On the other hand, in order to determine effective diffusivity of water vapor in crust region, equation 3.31 is proposed in the model. Nonetheless the simulation program determines effective diffusivity by Millington and Quirk [21] model. Relevant properties are also introduced in porous medium transport properties interface.

46

Adjacent boundaries of crust region are water interface and outermost droplet diameter. At water interface, i.e. R_w, equation 3.87 can be used with proper temperature, which will be determined in heat transfer modules as a dependent variable. R_d is the interface where mass transfer between vapor and ambient air takes place. Therefore a general outwards flux is introduced for R_d boundary and below equation is obtained

$$N_{wv} = -k_m(c_{wv} - c_{air})$$ (3.88)

where N indicates molar flux. Water vapor concentration present in ambient air is determined by considering humidity. The general equation used for $c_{wv,air}$ can be written as

$$c_{wv,air} = AH \times \frac{\rho_a}{M_w}$$ (3.89)

where AH is absolute humidity in units g water vapor per g air.

General characteristics for transport properties of water and vapor in the droplet are explained. These mechanisms mainly determine the vapor diffusion from crust region to ambient air and inner mass transfer operations, such as water concentration with changing porosity and vapor concentration with increasing concentration from evaporation front.

3.2.3. Heat Transfer Mechanism

Heat transfer in fluids module is utilized to simulate heat transfer operations taking place in the droplet. The domains 2 and 3 have same materials and physical properties

mentioned in transfer mechanism section. Other than that, additional properties are introduced and relevant interfaces are described for heat transfer mechanism.

For the slurry and shell regions, where liquid is present, porous media option is again enabled in physical model, in which porosity of corresponding region and properties of materials, both fluid and solid, must be indicated. Initial value for temperature is constant at ambient temperature for all regions. The volume fraction of solid particles in D2, very similar to the equation 3.83 describing averaged porosity as a variable in previous section, can be expressed as

$$\varphi_s = 1 - \left(\frac{V_{sl}}{V_{liq}} \varphi_w + \frac{V_{sh}}{V_{liq}} \varepsilon \right) \tag{3.90}$$

On the other hand, properties of the materials like thermal conductivity, density and heat capacity must be indicated in porous medium interface, hereby description of the domain, which will be exposed to heat exchange, is complete. The simulation determines effective thermal conductivity for the corresponding domain via volume averaging approach.

Adjacent boundaries to this domain are R_{vc} and R_w, whose temperatures are defined the same as temperature of D2 and D3, respectively. The reason that the temperature of water interface is equated to the temperature of dry crust region is to sustain thermal continuity between those regions. It is already mentioned that physics in vacancy region are ignored in this simulation.

One of the significant interfaces in this module is boundary heat source applied at water interface. The equation that expresses heat loss by evaporation at this boundary

is obtained by combining equation 3.39 and 3.62 in such a way that heat difference in conduction is written in terms of mass change of evaporated water, such as

$$\varepsilon \rho_w \lambda_w \frac{dR_w}{dt} = -k_{cr} \frac{\partial T_{cr}}{\partial r} + k_{sh} \frac{\partial T_{sh}}{\partial r} \qquad (3.39)$$

$$\varepsilon \rho_w \frac{dR_w}{dt} = M_w D_{cr} \frac{\partial c_{wv}}{\partial r} \qquad (3.62)$$

$$Heat\ loss = -\lambda_w M_w D_{cr} \frac{\partial c_{wv}}{\partial r} \qquad (3.91)$$

Simultaneity of the model begins to appear also in the simulation, since heat loss is determined by motion of evaporated water and water vapor concentration at evaporation front is determined by corresponding temperature. This example is only one of the connected operations throughout the model. As connections of dependent variables increase, so does the complexity of the solution.

Another dependent temperature is defined in heat transfer in fluids module for crust region, i.e. D3. Similar arrangements are done also for this module, such as introducing properties of vapor and solid in relevant fields, as well as indicating porosity of the medium. However, the porosity in this domain is constant for all times and expressed with ε.

At water interface, which is the inner boundary of D3, temperature as the dependent variable of this domain is equated to the temperature of D2. Exact opposite expression was introduced in the previous module. Other adjacent boundary however is where

convective heat transfer from ambient air takes place. Thus, a heat flux interface with external forced convection is introduced, in which required parameters such as droplet diameter, air velocity and air temperature are described. Although heat transfer coefficient can be calculated and entered manually, external forced convection module is preferred because it provides a more user-friendly interface.

The characteristics of heat transfer mechanism presented in the simulation are briefly summed up. As transport and heat operations take place as indicated, movements of boundaries must be also specified.

3.2.4. Motion of Boundaries

Physical changes in the structure of the droplet are simulated with motion of boundaries. For this operation, boundary ODEs module is used. As a reminder, R_w indicates the water interface, thus receding mechanism should be expressed in corresponding ODE. R_{sh} indicates shell inner boundary, although it does not appear as a structural boundary in the simulation, its value is calculated via an ODE, also constructed in model. Finally, R_{vc} indicates vacancy boundary, which moves towards the evaporation front after certain time interval. Since the droplet diameter remains constant in second stage of drying, no operation for R_d involves in this section.

To begin with, R_w is defined in its relevant module and the equation expressing R_w is derived from equation 3.62

$$\frac{dR_w}{dt} = -\frac{M_w D_{cr} \frac{\partial c_{wv}}{\partial r}}{\varepsilon \rho_w} \qquad (3.92)$$

Similar to heat loss from that boundary, motion of water interface can also be derived from equation 3.39, however in order to preserve consistency in utilized parameters R_w is written in terms of mass parameters. As initial value of above ODE, $R_{w,i}$ is introduced. Since the movement is towards the center, above equation necessitates a minus sign.

As another ODE R_{sh} is defined at water interface, for two reasons. One is that R_{sh} has actually no individual boundary structurally defined and second is that R_{sh} is strongly depending on R_w and defining it on R_w's boundary makes it a lot simpler to calculate. Otherwise, it would require an operator to use the value of differential term at the right hand side of below equation at another boundary. Even though R_{sh} is defined at somewhere else, its mathematical value is not affected of this condition. The condition that R_{sh} is moving is only valid as long as solid particles are present in slurry region. Thus,

For $\varphi_w < 1, t \geq 0$

$$\frac{dR_{sh}}{dt} = \frac{R_w{}^2}{R_{sh}{}^2}\frac{dR_w}{dt} \tag{3.93}$$

Since the change in R_w is in negative direction, so will be the change in R_{sh}. This situation becomes reversed in case of R_{vc}. The motion of vacancy boundary is defined at its own boundary with the condition that it moves after water volume fraction reaches one in slurry region. Equation for R_{vc} is obtained as

For $\varphi_w = 1, t \geq 0$

$$\frac{dR_{vc}}{dt} = \varepsilon\frac{R_w{}^2}{R_v{}^2}\frac{dR_w}{dt} \tag{3.94}$$

Initial conditions for equation 3.93 and 3.94 are $R_{sh,i}$ and $R_{vc,i}$ respectively. Dependency of motion of shell inner boundary and vacancy boundary on water interface makes all the interface movements also dependent on mass transfer operations occurring in crust region. So the simultaneity of the model once again appears in motion of boundaries module.

Until this point, ODEs for all three moving boundaries are described and carried out in the simulation. However, it is required to actually move these geometries, along with determining their mathematical solutions. Thus, deformed geometry module is utilized, where boundaries R_w and R_{vc} are assigned to move with a velocity of dR_w/dt and dR_{vc}/dt, as they are calculated in boundary ODE modules, towards and outwards from the center of the droplet, respectively.

3.2.5. Study Characteristics

All domains must be initially meshed with proper size options, where various meshing sizes may yield different end results as it is an important factor for convergence of the solution. Especially the boundaries where many physics are involved are supposed to have tight meshing structure.

Study settings are close to default, where a time dependent study is in action. The solution is expected to cease when the water domain becomes so thin that the simulation cannot calculate further, so there is no exact time range to set before executing the study. As ending time a relatively great parametric value is set according to expectations obtained from previous trials, besides an appropriate time step of choice is to be determined.

52

On the other hand, since there are changes in the geometry, an automatic remeshing interface is introduced in order to change and adapt the meshes to changing geometry. This interface provides a significant improvement to convergence ability of the study, since stable meshing would not be sufficient for the obtained geometry after certain time interval and would lead to errors. Additionally, in order to increase stability of the study, time stepping functions are utilized in some interfaces and besides some operators like averaging are also introduced at some points.

Study of the simulation gives concentration and temperature profiles for all regions except vacancy region, motion of boundaries R_w, R_{sh} and R_{vc} individually, and also variables like φ_w, on request. Additionally, it is possible to plot the change in certain variables with respect to time in a 2-D figure and also to track how meshing changes in time by simply plotting meshes in results section. As a conclusion, as long as all mechanisms are properly introduced and all physics are connected to each other, COMSOL provides a significant ease to solve the whole problem in very short times with accurate results.

CHAPTER 4

RESULTS AND DISCUSSION

4.1. Simulation Studies

A couple of studies are executed with various parameters switched in order to see related effects. Default parameters are determined through analysis of previous studies and appropriate values are chosen for the beginning of the second stage of drying. Initial study plays the role of a control study, whereas parameters like temperature, air velocity, humidity of air, droplet size and initial volume fraction of solids in slurry region are changed in subsequent studies.

Some of these parameters are mentioned numerically in this chapter as they describe the physical status of the corresponding study. The ones which are not mentioned in this chapter can be found in Appendix sections, where all parameters and properties are presented.

Discussion of tabulated results is held in each individual section, whereas comparison of obtained results with literature data and relevant discussions are done in a separate section at the end of this chapter.

4.1.1. Initial Study

Most of the parameters for initial study of the simulation are determined based on some of the parameters introduced in Nesic and Vodnik [6] and the results presented by Mezhericher et. al. [1], in which first stage of drying is investigated elaborately. It is stated that 2 mm diameter droplet with suspended SiO_2 particles undergoes a drying process and outcomes of the first stage of drying are demonstrated. Although properties like initial solid volume fraction, air temperature and velocity are not directly assumed as the same, presented results are rather considered as an appropriate initial condition for the second stage of drying.

According to previous model results [1], approximately 18% reduction is observed in droplet size just after the first stage of drying. Thus, for a droplet with a radius of 1 mm, this outcome would yield a final droplet radius of 0.82 mm for the first stage. It is noteworthy to mention once more, that no exact specification for the initial conditions for this simulation is sought; instead the point is just to specify rather reasonable values. Hence, the default droplet radius for initial simulation study will be 0.805 mm and values of other layers will be estimated based on this one. Since second stage of drying is initiated as soon as water interface recedes behind the outermost solid particles, i.e. droplet radius, it would be appropriate to set a value of 0.8 mm for $R_{w,i}$ as initial condition. As mentioned in previous sections, it is preferable to leave a decent distance between these two boundaries in order not to tighten the mechanics taking place in that region. Another initial parameter to be specified is shell inner boundary, which is simply rounded and set as 0.6 mm, based on the given data in relevant paper [1] that shell thickness to droplet radius ratio is around twenty-ish percent at the end of first stage. Finally, a vacancy region is formed with a very small value for initial condition, namely 0.01 mm.

Another parameter, which is set based on the results presented in aforementioned paper, is porosity of solid particles in shell and dry crust regions. It is stated that 0.6 is the maximum theoretical value for orthorhombic packed spheres according to Rumpf [22], thus value of ε for these regions will be 0.4 for all times. On the other hand, as a parametric value water volume fraction in slurry region is assumed as 0.75 initially, although smaller values are also discussed in previous studies.

The initial temperature throughout the droplet is set to wet-bulb temperature of air according to its dry-bulb temperature and humidity of the ambience, which is at the same time the ambient temperature during the whole process. In the meantime air temperature and velocity are set to 340 K and 0.5 m/s, respectively. Another important property of air is humidity, which is one of the parameters affecting evaporation rate of water. Absolute humidity of air is set to 0.01 g water vapor/g air as a default condition, which in the meantime corresponds to approximately 5.8% relative humidity for a dry-bulb temperature of 340 K (see Appendix C). Regarding these data, wet-bulb temperature of air is determined as approximately 302 K, which is introduced as initial droplet temperature for the second stage of drying. Even though air temperature is set as mentioned, properties of air are considered at average film and ambient temperature (see Appendix A). The effect of pressure is not included into the simulation and its value is set to 1 atm as default. Besides, some other properties that are present in the simulation as default are left as they are.

As mentioned, various properties of water, air, solid and water vapor and also required coefficients are presented with relevant references in Appendix section and also how they are obtained if any calculation is necessary.

Results of drying simulation are tabulated for three different stages, namely initial condition, time of vacancy emergence i.e. depletion of solids in slurry region and final condition. Concentration of water vapor at evaporation interface, temperature of both domains –average for liquid domain, outer boundary for crust region- and also values of the boundaries are presented in these tables for the corresponding stage. Additionally, plots for temperature, amount of water and motion of boundaries with respect to time are presented, thereafter concentration and temperature profiles are demonstrated in Appendix D section at initial, half and final times of the drying process, in order to provide a general overlook to the morphological change of the domains.

Note that data for temperature of water is given as an average value since it does not vary considerably along its individual domain. Although temperature values of both domains are very close to each other, temperature of crust boundary is also presented in the results table. On the other hand concentration of water vapor data is given at water interface, as it constantly increases along with evaporation process and there is a significant concentration gradient along the dry crust region.

Table 4.1. *Results for the main parameters of initial study*

Parameter	Unit	$t_{initial}$	t_{vc} (18.2s)	t_{final} (93.7s)
T_w	K	302	310.7	323.1
T_{cr}	K	302	311.0	323.6
c_{wv}	mol/m^3	1.58	2.51	4.58
R_d	m	8.05×10^{-4}	8.05×10^{-4}	8.05×10^{-4}
R_w	m	8×10^{-4}	7.5×10^{-4}	5×10^{-4}
R_{sh}	m	6×10^{-4}	5×10^{-4}	5×10^{-4}
R_{vc}	m	10^{-5}	2×10^{-5}	4.9×10^{-4}

Table 4.1 presents a general look at the results of initial study. It takes approximately 94 seconds for complete drying of the droplet with an initial water volume fraction of 0.75. As expected, water vapor concentration at evaporation interface increases continuously as temperature of that boundary increases. Figure 4.1 depicts temperatures of crust and inner wet regions with respect to time. Initial rapid increase of temperatures are followed by relatively slow increase. Furthermore the difference between the temperatures is initially negligible and it gets higher as evaporation proceeds. All these characteristics fit well with the formation and growth of dry crust region that introduces thermal resistance. At this point it is important to mention that ambient air temperature, T_a, and heat transfer coefficient, h, remain constant during the whole process, since air and droplet parameters in equation 3.18 is assumed as constant at an average temperature, presented in detail in Appendix A section.
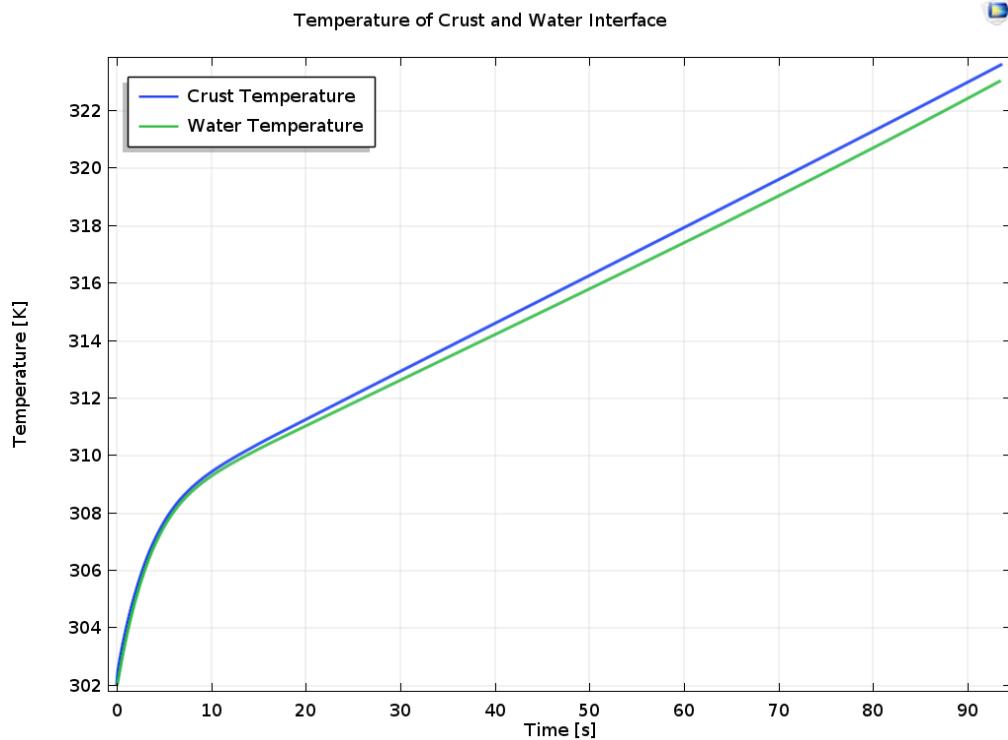
Figure 4.1. Temperature vs time plot for the initial study

59
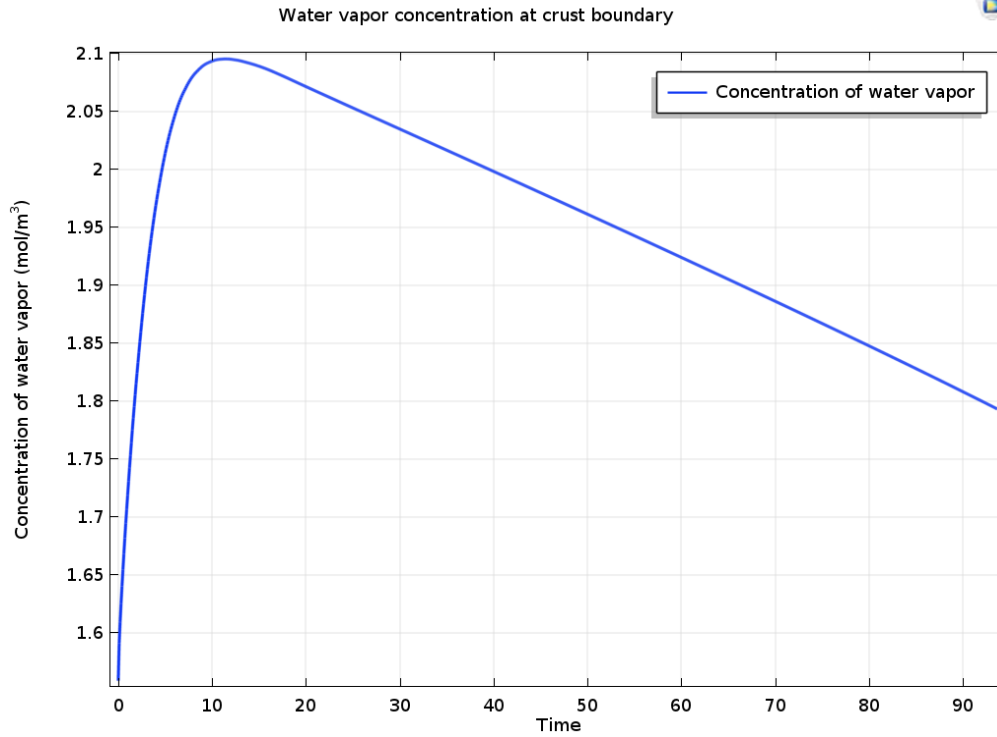
Figure 4.2. Vapor concentration vs time plot for the initial study

Water vapor concentration at evaporation interface initially increases sharply as shown in Figure 4.2. That increase however eventually slows down and then almost constant rate decrease is observed. The behavior of the interphase vapor concentration is directly affected by the individual temperatures of the crust and slurries. As those temperatures increase at the same rate, so does the vapor concentration. But as the water temperature falls behind the crust temperature, vapor pressure increase at the interphase will not compensate the negative impact of the lower temperature of the water through equation 3.52.
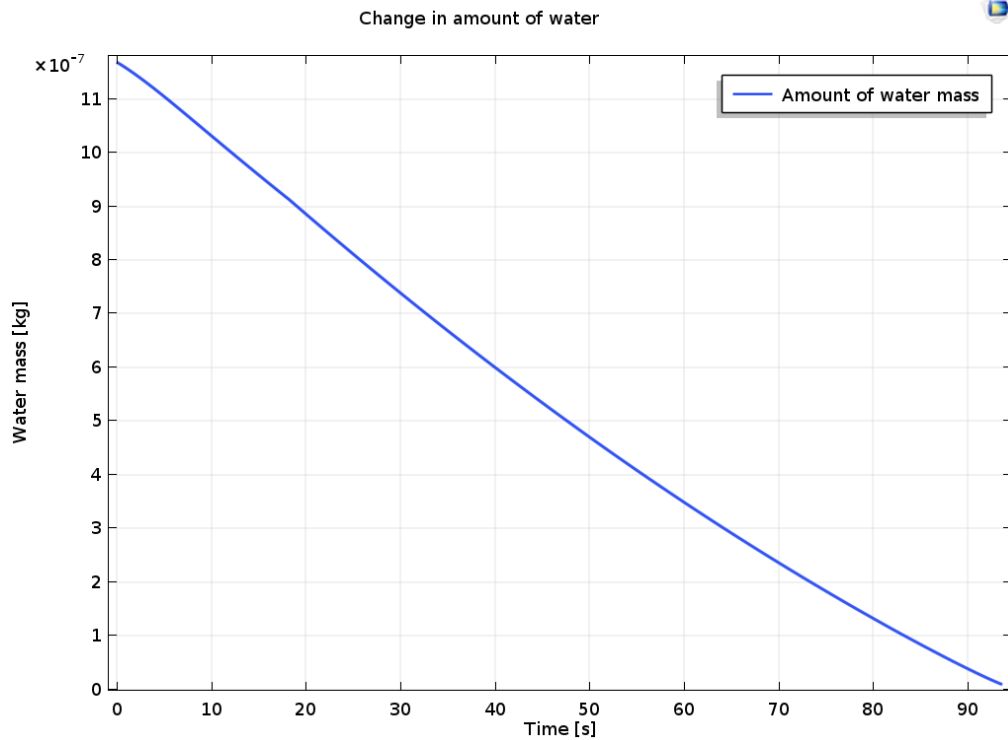
Figure 4.3. Amount of water vs time plot for the initial study

Amount of water, which is decreasing continuously as evaporation takes place, is plotted in Figure 4.3. At first the decrease trend of water amount seems quite constant. Nevertheless it is observable that there is a slight slowdown in water loss, in other words evaporation rate, especially in later time intervals of drying process, caused by decreasing heat flux and also mass and heat transfer resistances introduced again as thickness of crust region increases. This is the main reason for that second stage is called as falling rate stage, even though it is a very small change in evaporation rate due to the small dimension of the droplet.

Apart from that, when Figure 4.1 and 4.3 are analyzed together, it can be clearly observed that the rapid initial temperature increase and subsequent slowdown in the

61

temperature profile are not reflected into the evaporation rate, which is demonstrated in Figure 4.3. This discrepancy shows that the amount of heat, which is lost to evaporation and utilized to heat up the particle, varies in the course of time due to certain morphological changes of the particle and emerging heat and mass transfer resistances.
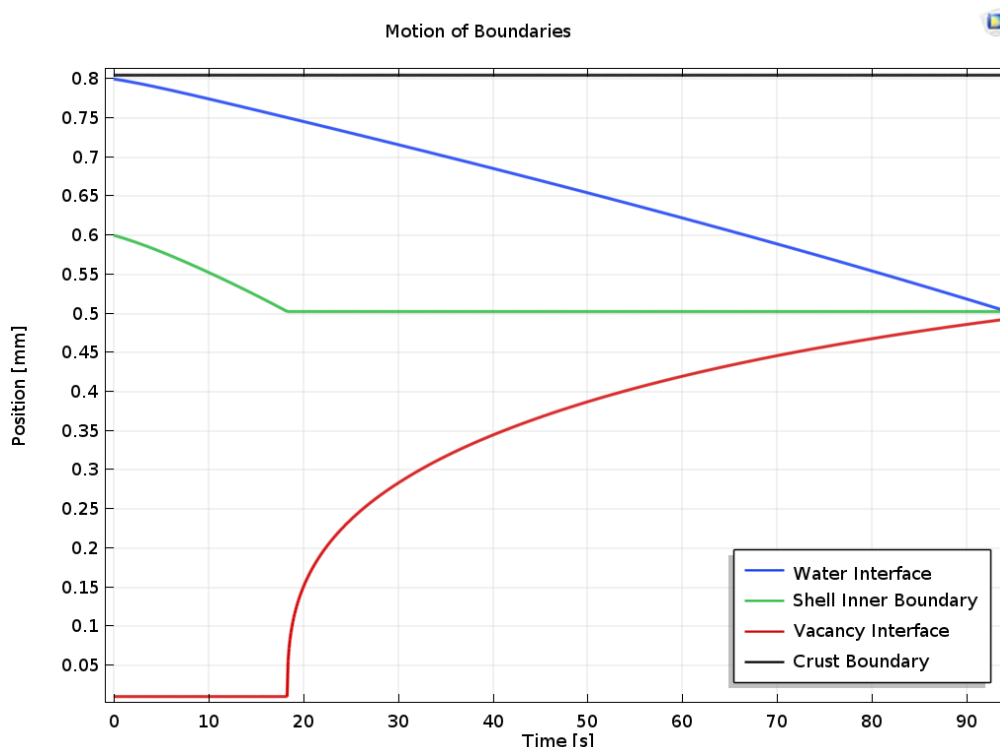
Figure 4.4. Boundary dimensions vs time plot for the initial study

Water and vacancy interfaces move towards each other as long as evaporation and diffusion operations occur. The motion of vacancy boundary is very high at t_{vc} because of huge R_w^2/R_{vc}^2 ratio, thus R_{vc} shows a significantly great initial expansion. Time for vacancy emergence is given with one decimal after comma, thus expressed t_{vc} instant only presents the approximate instant for that incident. In other words, at t=18.2s water

volume fraction has just approached to one, therefore it can be stated that emergence of vacancy occurs at a time between 18.1-18.2s. As can be observed in Figure 4.4, from that instant on vacancy region grows and shell inner boundary remains constant. Water and vacancy interfaces collide in a location very close to shell inner boundary. Although there is a small difference between the final values of R_w and R_{vc}, this can be considered as a small convergence error, probably caused by averaging operators used in boundary ordinary differential equation modules. Besides it is nearly impossible to equate a domain to zero in such simulations, thus a complete convergence is not expected after all.

By using the initial and final values of boundary dimensions, it can be proved that solid particles inside the droplet remains the same throughout the drying process via a mass balance operation. Equation 3.95 is a simplified version of the mass balance for the solid particles, equating the initial and final amounts, respectively.

$$\left(R_d{}^3 - R_{sh,i}{}^3\right)(1 - \varepsilon) + \left(R_{sh,i}{}^3\right)(\varphi_s) = \left(R_d{}^3 - R_{sh}{}^3\right)(1 - \varepsilon) \qquad (3.95)$$

$$[(8.05x10^{-4})^3 - ((6x10^{-4})^3](1 - 0.4) + [(6x10^{-4})^3](0.25)$$
$$= [(8.05x10^{-4})^3 - (5x10^{-4})^3](1 - 0.4)$$

$$2.37x10^{-10} = 2.38x10^{-10}$$

As also mentioned in previous sections, at the initial stages of the second stage solid particles are present in the shell region with a closely packed formation and in slurry region with a significantly lower fraction. Receding of shell boundary ceases when all solid particles adhere to the shell and solid particles gather in both shell and dry crust regions with a constant porosity, ε. Thus, equating these two conditions would yield

the same amount of solid. Above calculation proves that the results presented by the simulation abide by conservation of mass of solid particles during the drying operation.

Profiles for concentration of water and water vapor, average temperature of water and crust region are demonstrated below, in order to observe the morphological evolution of the droplet. Illustrations include the profiles for three time steps, namely initial, half and final times of drying.
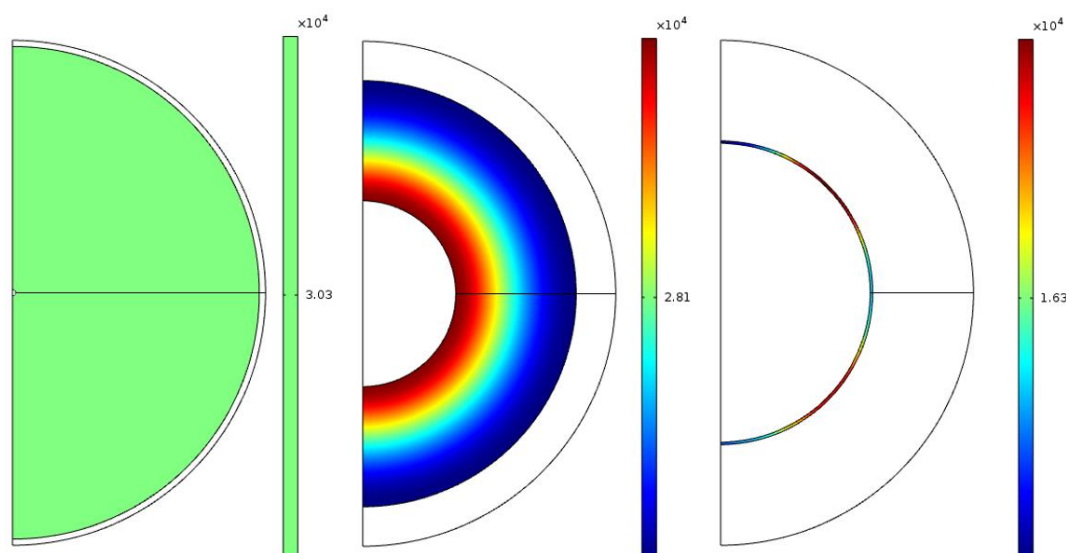
Figure 4.5. Spatial profile of water concentration

During the drying process the droplet undergoes a morphological change, where liquid domain shrinks and crust region thickens. In Figure 4.5, concentration of water is illustrated with the structural appearances at initial, half and final moments of the initial study in mol/m^3. The concentration of water is initially uniform throughout the droplet. However, in subsequent stages transfer of water molecules in the slurry region

can be observed with a very slight distribution. Although the concentration gradient is significantly low, this figure gives a main idea for the behavior of liquid water in the droplet.

On the other hand, the concentration of water vapor can be observed in the dry crust region. Figure 4.6 demonstrates the evolution of the crust region and concentration gradient of water vapor particles. Evaporated water diffuses through the crust to the ambient air, occupying the whole pores of the domain. Apparently, the concentration gradient increases gradually, as temperature of the particle and the amount of water vapor increases.
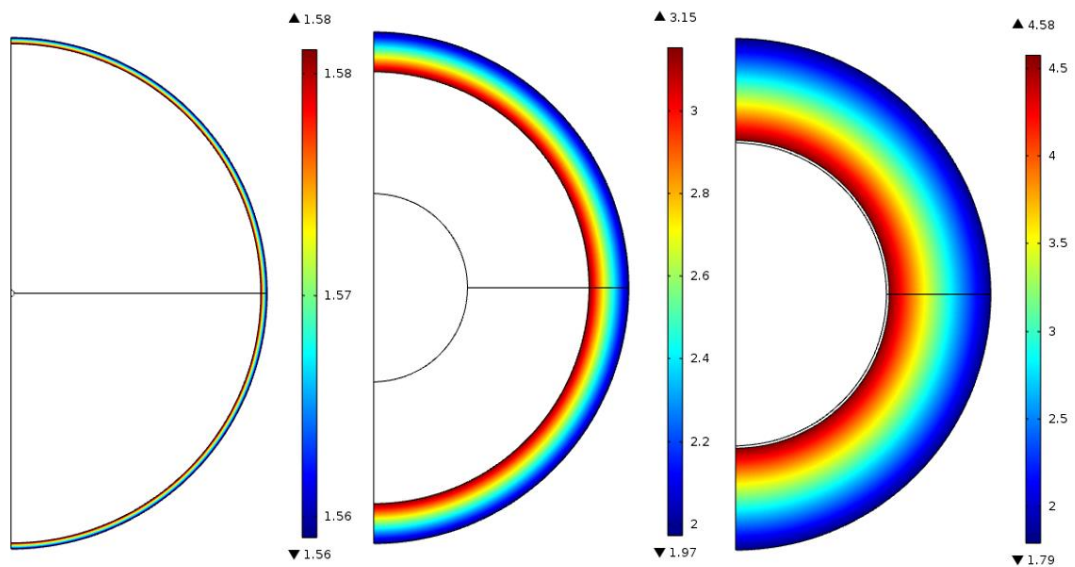
Figure 4.6. Spatial profile of water vapor concentration
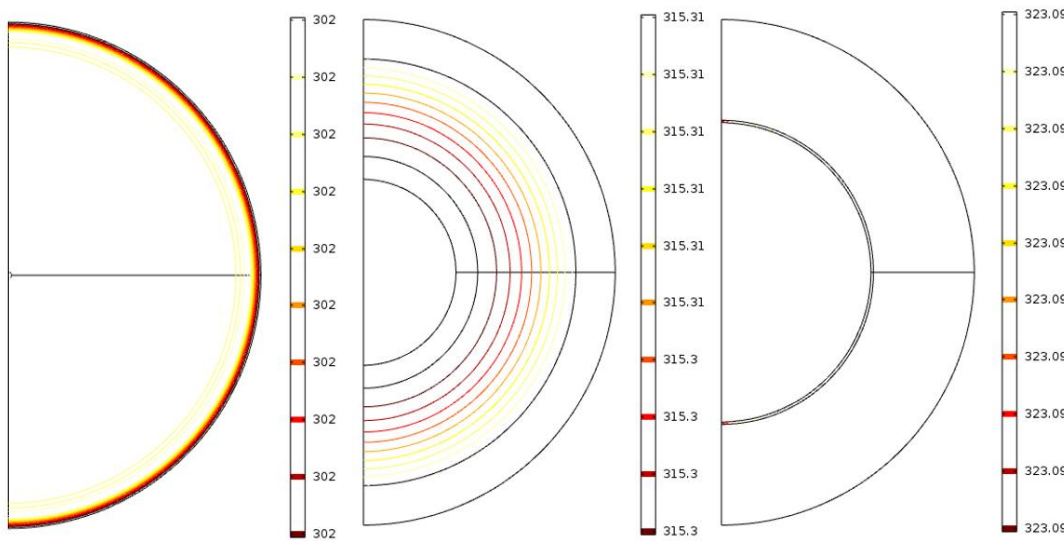
Figure 4.7. Spatial profile of water temperature

Temperature of the droplet is increasing constantly, nevertheless temperature gradient in both watery (slurry and shell) and crust regions is substantially low, shown as temperature contours in Figure 4.7 and 4.8 in Kelvin. The figures provide a coherent view about how temperature is conducted to the inner regions of the droplet.

One of the main results that can be drawn from spatial temperature profile plots is that the temperature distribution in crust region has a broader range in comparison to one in slurry and shell regions. That means heat is transferred through the crust region as it loses some of its energy by increasing the temperature of that specific location, resulting a heat resistance in the way. On the other hand, as heat is further conducted to water interface, most of it is lost by latent heat of evaporation.
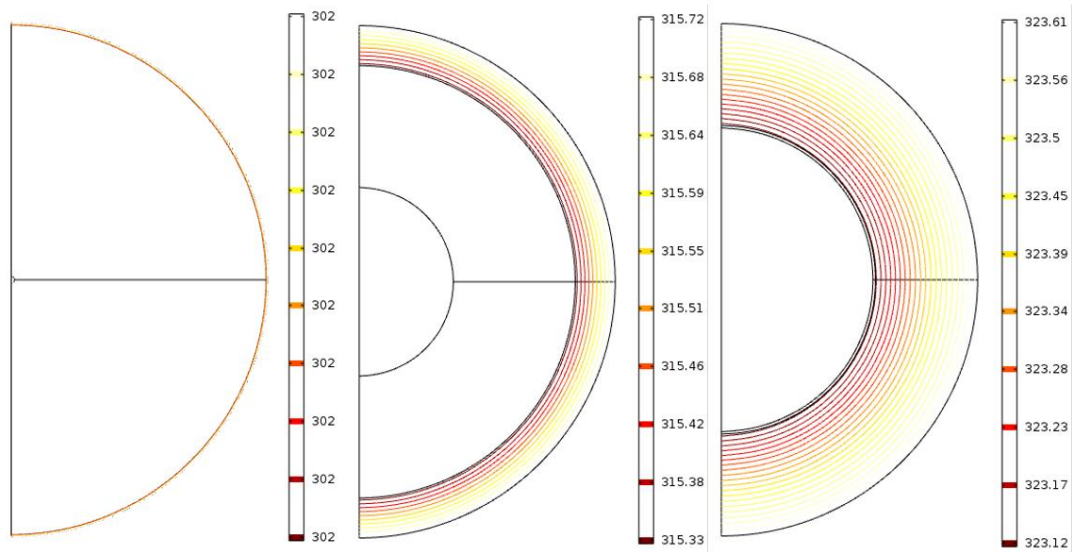
Figure 4.8. Spatial profile of crust temperature

Another point requires mentioning at this step is the role of the assumptions in the model, simulation and obtained results. First, the model and also the simulation are incapable to determine any scenario including particle breakdowns or ruptures due to extreme conditions or any disruption in the particle morphology, since the assumptions such as spherical droplet shape, radial movements and ignored effects of directional air flow support the model as they simplify the calculations on the other hand. Besides, constant property assumption for the materials can also lead to results differentiating from the real case. For the sake of simplification, these kinetics are left out of the scope of this study and aforementioned assumptions are taken into consideration.

Calculations are carried out by the simulation program until a point where convergence problems arise. As simulation stops the calculation process, it is assumed

that instant is the final time for the process and maximum convergence for adjacent boundaries of liquid domain is achieved.

As mentioned at the beginning of this section, some of the parameters are kept changing in order to analyze their effects on drying process. Studies executed by varied parameters are presented in subsequent sections. Nevertheless, concentration and temperature profiles are not necessarily plotted for each consecutive study, since the general profiles of those are very similar to the ones that are already demonstrated for initial study, except simulation times. Results are however tabulated similarly and discussed.

4.1.2. Effect of Increase in Air Temperature

Other parameters remaining same, temperature of flowing air is increased to 370 K, so that the effect of high temperature can be investigated. Corresponding wet-bulb temperature is determined as approximately 308 K. Besides, assumed humidity ratio of 0.01 g water vapor/g air corresponds to approximately 1.75% relative humidity at this temperature. Since temperature of air is higher, it is expected that particle will be heated up more quickly in comparison to initial study, and also final temperature will be higher. The properties of air are estimated for a relatively higher temperature value in this particular study, namely 350 K as a rough average of crust and ambient temperatures, corresponding effects are not quite observable for mass transfer operations, since mass transfer coefficient does not show significant change with respect to temperature. However, heat transfer coefficient is approximately 10% higher than the initial study (see Appendix B).

Table 4.2. *Results for the main parameters of the study with increased temperature*

Parameter	Unit	$t_{initial}$	t_{vc} *(10.8s)*	t_{final} *(51.8s)*
T_w	K	308	319.7	336.8
T_{cr}	K	308	320	337.9
c_{wv}	mol/m^3	2.18	3.91	8.42
R_d	m	8.05×10^{-4}	8.05×10^{-4}	8.05×10^{-4}
R_w	m	8×10^{-4}	7.5×10^{-4}	5×10^{-4}
R_{sh}	m	6×10^{-4}	5×10^{-4}	5×10^{-4}
R_{vc}	m	10^{-5}	10^{-5}	4.9×10^{-4}

Instantly observable that the overall duration for drying has been reduced almost to its half in comparison to initial study, same argument is also valid for the time when vacancy region emerges. As expected, droplet dries quicker at high temperatures. Temperatures of both domains are very close to each other, however in comparison to previous case, temperature values of water and crust regions are more clearly distinguished from each other in this case as shown in Figure 4.9. Primary reason for this is simply higher gradients associated with the higher outer temperature.

Since evaporated amount increases at high temperatures, so does the concentration of water vapor as it is directly proportional with temperature. Water vapor constantly diffuses through crust and eventually to ambient air, similar to the initial study, there is a significant concentration gradient in dry crust region. Although the concentration difference between adjacent crust boundaries are much greater when air temperature is high, this situation is not caused by different mass transfer coefficients, instead by high concentration of water vapor present in the second case. The comparison of water vapor profiles of the first two cases is illustrated in Figure 4.10.

The decrease trend in water amount is very similar to the initial study, however in this case complete evaporation of water occurs in a shorter time interval. Besides motion of the boundaries follow almost the same pathway as the initial study, therefore these plots are not demonstrated individually.
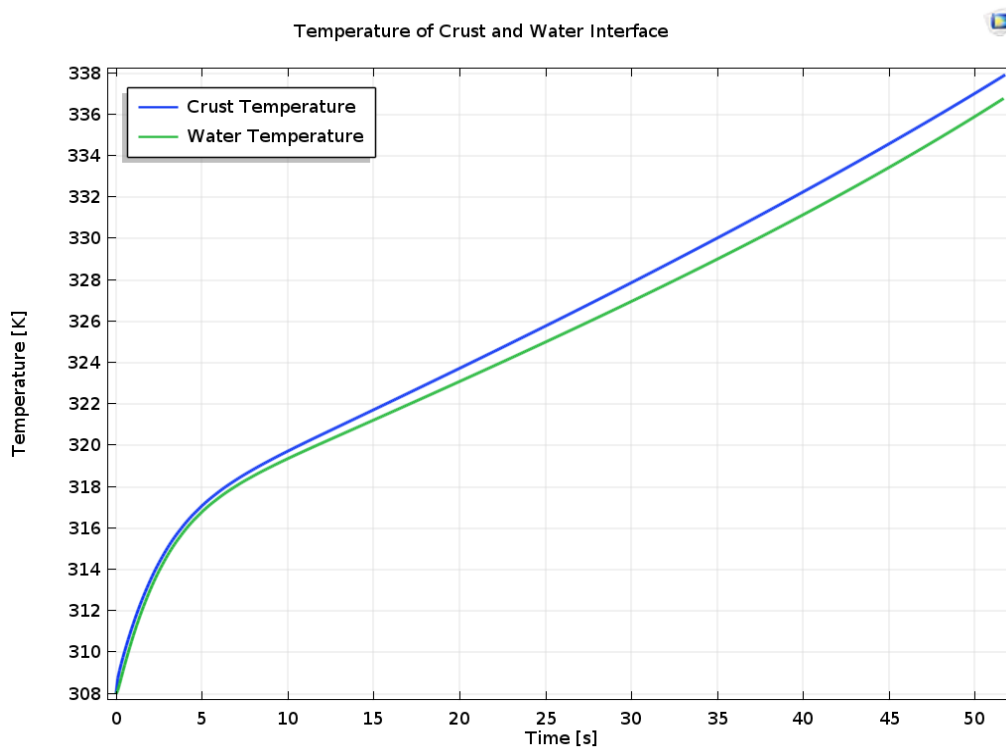
Figure 4.9. Temperature vs time plot for the study with increased air temperature

Since the conditions at t_{vc} are quite similar for all studies, status of the boundaries at that instant is also expected to be very close in each case. Only small differences may be observed for R_w in terms of boundary dimensions in particular studies with different parameters, whose motion depends on evaporation rate. Estimated dimensions of all interfaces are quite reasonable for this particular case, dismissing the fact that some convergence constraints are at hand at final situation. It is assumed that the

70

evaporation process is almost complete, because the thickness of liquid domain is very small.
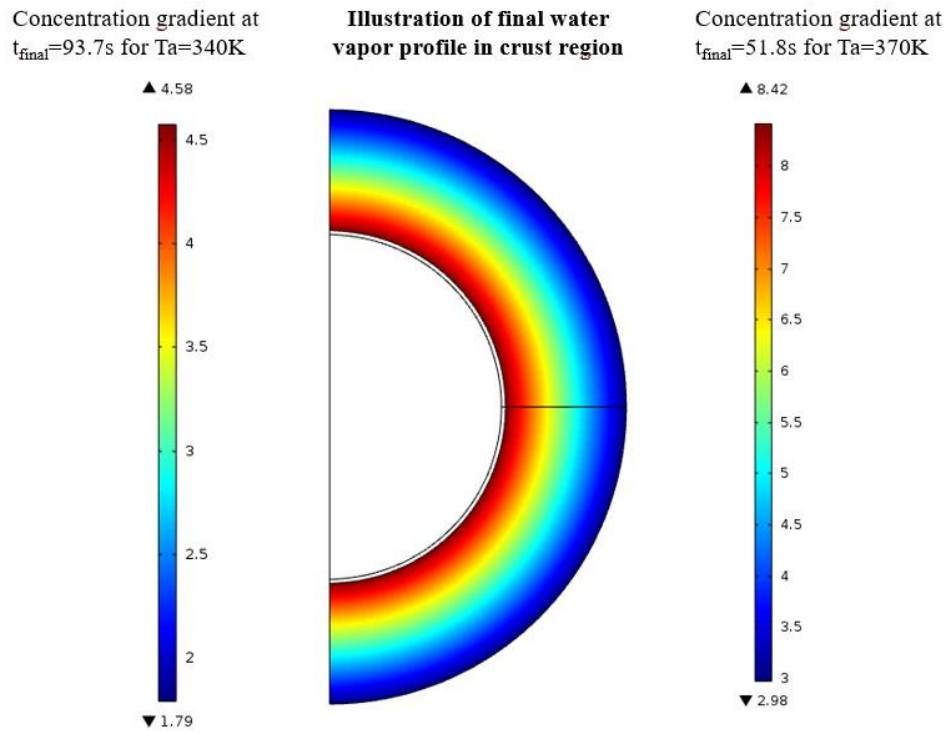
Figure 4.10. Concentration distributions of water vapor in crust region for the studies with different air temperature values

4.1.3. Effect of Increase in Air Velocity

The velocity of air is increased to 1 m/s in order to see the effect of air velocity on drying process. In this particular study, only parameter that is different from default values is air velocity. That means temperature of air is again set back to 340 K. Velocity of air affects both convective heat transfer coefficient and mass transfer coefficient, which are expressed in equations 3.18 and 3.27, respectively. Therefore it is expected to see differences in received heat from ambient air and as well as diffusion of water vapor profile in crust region.

Drying operation with increased velocity seems to be occurring relatively faster in comparison to the initial case. Approximately 17 seconds of reduction in drying time is observed by doubling the velocity of air. Relevant data are tabulated below,

Table 4.3. *Results for the main parameters of the study with increased velocity*

Parameter	*Unit*	$t_{initial}$	t_{vc} *(14.5s)*	t_{final} *(76.9s)*
T_w	K	302	311.0	324.3
T_{cr}	K	302	311.3	324.9
c_{wv}	mol/m^3	1.58	2.55	4.84
R_d	m	8.05×10^{-4}	8.05×10^{-4}	8.05×10^{-4}
R_w	m	8×10^{-4}	7.5×10^{-4}	5.1×10^{-4}
R_{sh}	m	6×10^{-4}	5×10^{-4}	5×10^{-4}
R_{vc}	m	10^{-5}	10^{-5}	4.9×10^{-4}

Temperature of the particle at t_{final} is very slightly higher than the final temperature of initial study. This is a quite considerable outcome for a drying process with higher air velocity. Additionally these temperature values are obtained even in a shorter time interval, because of an increase in heat transfer coefficient introduced by higher air velocity.

On the other hand, because of higher mass transfer coefficient the difference in the concentration gradient of water vapor increases up to values such as 3.18 mol/m^3 (4.84 at evaporation front; 1.66 at crust boundary) whereas this difference is 2.79 mol/m^3 for initial case. That means water vapor has higher mobility in crust region when air velocity, and mass transfer coefficient accordingly, are higher.

There is no remarkable change in the final morphology of the particle and its inner layers. Rate of water loss and motion of the boundaries again possess similar trend as Figure 4.3 and 4.4, except the fact that drying duration is shorter.

4.1.4. Effect of Increase in Humidity

Absolute humidity of air is increased to 0.02 g water vapor per g air from 0.01, corresponding to approximately 11.3% relative humidity and a wet-bulb temperature of 307 K (see Appendix A and C). Thus, concentration of water vapor in ambient air is greater in this case. With such a change in humidity, an effect in mass transfer rate of water vapor is expected, since one of the key parameters determining this rate is the difference between concentration of water vapor at outermost droplet boundary and at ambient air. Hence, although mass transfer coefficient is the same as default condition, concentration difference comes into play at this point. Corresponding mass transfer equation was given in equation 3.49.

The results are presented in Table 4.4. In comparison to the initial case, it can be seen that drying process takes slightly more time when humidity is greater. Main reason for such a delay is the reduction in the mass transfer driving force due to the increased ambient air humidity. Reminding that when the relative humidity of air is one, then there would be no evaporation of water, instead particle would only be heated up.

Table 4.4. *Results for the main parameters of the study with increased humidity*

Parameter	Unit	$t_{initial}$	t_{vc} (20s)	t_{final} (100.2s)
T_w	K	307	313.8	324.0
T_{cr}	K	307	314.0	324.5
c_{wv}	mol/m^3	2.07	2.92	4.77
R_d	m	8.05×10^{-4}	8.05×10^{-4}	8.05×10^{-4}
R_w	m	8×10^{-4}	7.5×10^{-4}	5.1×10^{-4}
R_{sh}	m	6×10^{-4}	5×10^{-4}	5×10^{-4}
R_{vc}	m	10^{-5}	2×10^{-5}	4.9×10^{-4}

Since overall duration is greater, droplet is exposed to hot air for a greater time interval with similar heat transfer properties. Therefore final temperatures of liquid and gaseous domains are also higher than initial case. Regarding this, water vapor concentrations are relatively high at water interface, and it should also be mentioned that diffusion of water vapor particles from crust region are relatively slow. The slowing mechanism is, as also mentioned before, smaller difference between water vapor concentrations at crust boundary and ambient air, introduced by high relative humidity. That results in a narrower concentration gradient in crust region, which can be observed in Figure 4.11. It is obvious that water vapor particles leave the outermost boundary of the particle slower, where the concentration difference between water

interface and outer crust boundary is approximately 2.45 mol/m^3, when the humidity of air is even a little greater. This difference was estimated as 2.79 mol/m^3 for the initial study.
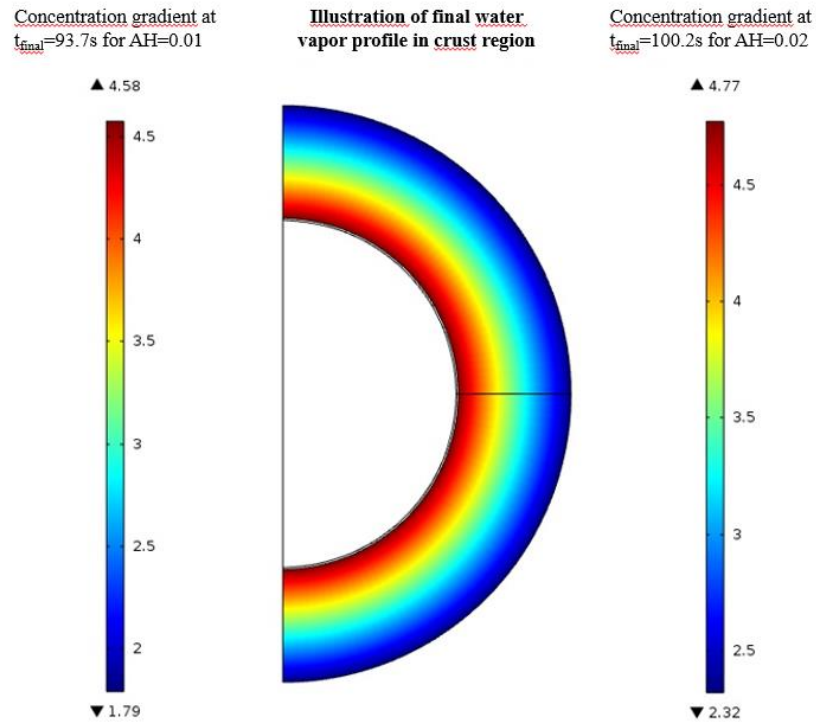

Figure 4.11. Concentration distributions of water vapor in crust region for the studies with different humidity values

In summary increased humidity causes slower mass transfer rate for water vapor and consequently slower evaporation of water, resulting in longer drying time interval and denser vapor phase in crust region.

4.1.5. Effect of Increase in Droplet Size

Size of the droplet is doubled including the layers within, in order to see how a relatively bigger droplet undergoes second stage of drying. Dimensions of inner layers can also be arranged with different increments, however the assumptions taken into consideration while determining the default structural ratios of the droplet are also valid for this trial. Different ratios of inner boundaries are not included in the scope of this study.

The heat and mass transfer mechanisms are expected to change a fair amount, since droplet size plays a significant role in estimation of convective heat and mass transfer coefficients. On the other hand, since amount of water is much greater in current conditions, it would take for sure a much longer time to dry the whole particle.

Initial value set for vacancy boundary, i.e. R_{vc}, however is not changed, because that boundary is initially there only for removing the need of dividing the study into two steps. Results for the main parameters are presented in Table 4.5.

Drying time increased significantly for a double size droplet, with a complete drying duration of approximately 305s. In relation to that, emergence of vacancy occurs also relatively later, at approximately t=58s. Temperature of water and crust boundary show very slight changes in comparison to initial case (Fig 4.12). There is only a temperature difference of 1-2 K, even if the droplet is exposed to hot air for a duration more than threefold of the initial case. The fact that temperature of the droplet does not differentiate much, proves on the other hand that most of the heat received is lost by evaporation. Heat and mass transfer coefficients are reduced almost to their half values, therefore slowing the diffusion of water vapor from the water interface and

76

reducing received amount heat by the droplet. In addition larger droplets have smaller surface to volume ratio. Therefore much higher drying time can be expected as the droplets get larger.

Table 4.5. *Results for the main parameters of the study with increased droplet size*

Parameter	Unit	$t_{initial}$	t_{vc} (58s)	t_{final} (305.1s)
T_w	K	302	311.0	324.2
T_{cr}	K	302	311.3	324.8
c_{wv}	mol/m^3	1.58	2.55	4.82
R_d	m	1.61×10^{-3}	1.61×10^{-3}	1.61×10^{-3}
R_w	m	1.6×10^{-3}	1.5×10^{-4}	1.02×10^{-4}
R_{sh}	m	1.2×10^{-3}	1.01×10^{-4}	0.98×10^{-4}
R_{vc}	m	10^{-5}	10^{-5}	0.97×10^{-4}

The concentration profile of water vapor seems however not affected that much since the temperature values throughout the droplet shows very similar regime as the temperature values of initial case. Nevertheless the concentration gradient in that domain is greater in this case, specifically 3.16 mol/m^3, probably because of the higher temperature gradients.

Final dimensions of the boundaries are close to twofold value of their initial results, so there is no significant change in receding and expanding mechanism of these interfaces, as trend of the boundaries remain the same. A small amount of difference between water interface and vacancy boundary still exists, resulting in a residual surface filled with water, because of convergence issues of the simulation study.
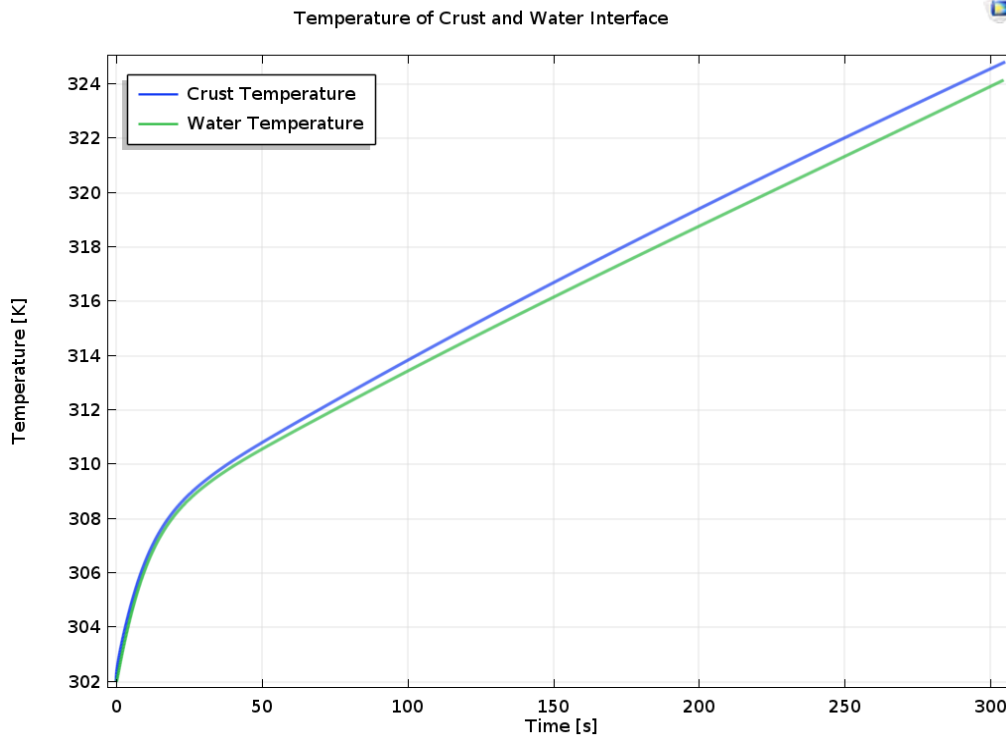
Figure 4.12. Temperature vs time plot for the study with double sized dimensions

4.1.6. Effect of Increase in Initial Solid Volume Fraction

Initial solid/water volume fraction of the slurry region is one of the most important parameters in this model, because as this value changes various mechanisms would also process in a different scenario as well as the morphological structure of the droplet. In the initial case, solid volume fraction in slurry region was set to 0.25, hence $\varphi_{w,i}$ was 0.75. For this particular simulation case, $\varphi_{w,i}$ is reduced to 0.65, meaning that initially denser slurry region is present at solid volume fraction of 0.35. Since the amount of solid particles inside the droplet is increased, then it is naturally expected to obtain a thicker shell at the end of the drying process.

Table 4.6. *Results for the main parameters of the study with increased solid volume fraction*

Parameter	Unit	$t_{initial}$	t_{vc} (25.3s)	t_{final} (93.3s)
T_w	K	302	311.9	323.1
T_{cr}	K	302	312.2	323.5
c_{wv}	mol/m^3	1.58	2.66	4.59
R_d	m	8.05×10^{-4}	8.05×10^{-4}	8.05×10^{-4}
R_w	m	8×10^{-4}	7.3×10^{-4}	5×10^{-4}
R_{sh}	m	6×10^{-4}	4.5×10^{-4}	4.5×10^{-4}
R_{vc}	m	10^{-5}	10^{-5}	4.7×10^{-4}

Actually since there are slightly less water molecules in the droplet, drying process is expected to be completed quicker. However as expressed in Table 4.6, time required to dry the droplet is almost the same as the default case. A significant increase of 7 seconds on the other hand can be observed for the instant of vacancy emergence, i.e. depletion of solid particles in slurry region. This is considerably reasonable because of an increase in initial solid amount. Regarding the time intervals for almost complete drying are quite same for both studies with 0.75 and 0.65 initial inner water fractions, such an interpretation can be put forward that even though diffusion and adhering of solid particles to the inner shell interface last longer, this delay is compensated by the time reduction provided by decreased initial amount of water and accordingly shifting the final time of the overall drying process to its initial value again.

This idea may be clarified and supported in terms of structural variables. As solid fraction increases in the slurry region of the droplet, time required for the depletion of solid particles increases, therefore R_{sh} ceases moving towards the center at a relatively later instant. Accordingly a delay for the emergence of vacancy arises. Nevertheless

the receding of water interface processes as it used to, as long as evaporation takes place. Besides, the evaporation process, i.e. convergence of two boundaries of liquid domain, is dependent neither on the water/solid fraction nor the motion of shell inner boundary. Therefore vacancy boundary moves upwards passing through the shell inner boundary, meaning that the interfaces of liquid domain would collide at a surface quite above this interface (Fig 4.13). Unfortunately a close convergence of adjacent boundaries of liquid domain similar to previous studies cannot be satisfied in this study.

The expectancy of a thicker shell is fulfilled by motion of inner shell boundary, where R_{sh} recedes back more than it does when water volume fraction was 0.75. Increasing solid fraction by 10% yields a shell thickening of approximately 5×10^{-5} m.

Temperature data do not show significant differences in comparison to initial case. A comprehensible outcome since the conditions for heat transfer are quite similar. Only difference is caused by average thermal conductivity coefficient in slurry region, which has an ignorable effect on the heat transfer through crust and shell region.

It can be concluded that the change in slurry volume fraction does not affect heat transfer mechanism and the migration rate of water molecules, but the depletion duration and shell characteristics.
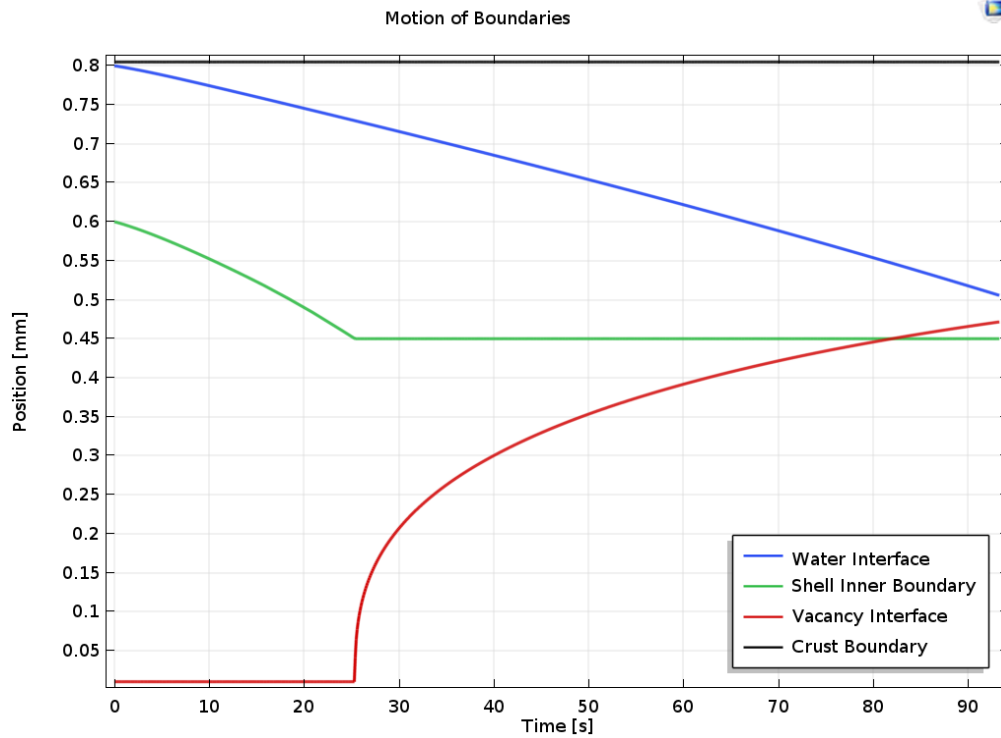
Figure 4.13. Boundary dimensions vs time plot for the study with increased initial solid fraction

4.1.7. Experimental Comparison Study

Numerous articles in this topic take the experimental results presented by Nesic and Vodnik [6] as reference source for the basis of their models. Thus, a reasonable adjustment in simulation parameters, which approximates the experimental conditions utmost, provides the opportunity to compare simulation study results with results of several articles at once that are also based on the same conditions. Therefore initial parameters such as air temperature and velocity are updated to 374 K (app. 101 °C) and 1.73 m/s, respectively.

81

Table 4.7. *Results for the main parameters of the experimental comparison study*

Parameter	Unit	$t_{initial}$	t_{vc} (8.3s)	t_{final} (37.2s)
T_w	K	308	326.6	344.2
T_{cr}	K	308	327.1	345.0
c_{wv}	mol/m^3	2.18	5.40	11.4
R_d	m	8.05×10^{-4}	8.05×10^{-4}	8.05×10^{-4}
R_w	m	8×10^{-4}	7.5×10^{-4}	5×10^{-4}
R_{sh}	m	6×10^{-4}	5×10^{-4}	5×10^{-4}
R_{vc}	m	10^{-5}	10^{-5}	4.9×10^{-4}

When both air temperature and velocity are increased, a significant increase in final droplet temperature and a considerable decrease in overall drying duration can be observed, as expected. On the other hand, high temperature leads to higher vapor concentrations at evaporation interface and also to a larger concentration distribution through the crust region.

In the next section, comparison with literature data is demonstrated and discussed not only for the results presented in this particular comparison study; but also for the cases, where the conditions of other conducted studies have resemblance to a previously published article.

4.2. Comparison of Results with Literature Data

There are various studies about experiments and models of drying kinetics of a nanosuspension droplet in the literature. Most of them includes a 1-2 mm diameter droplet with silica nanoparticles inside. The experimental results intrinsically involve both first and second drying stages as the droplet dries. Therefore modeling studies focus on the whole drying process in general, where kinetics and mechanism of the stages are investigated individually.

Similar to most of the papers in the literature, this thesis work also investigates modeling of the both first and second stages of drying, however it differentiates in a particular section. Although modeling approach shows similarity to previous works in this field, simulations executed in this study focus only on the second stage by utilizing a simulation program, COMSOL, which is capable to simulate almost any physical and chemical process in many fields as long as the model is defined properly. Therefore, instead of analyzing free evaporation process of a droplet, which has been already investigated many times, initiation of this simulation is set as the beginning of the second stage.

There are mainly two parameters to be compared with literature data, namely temperature and mass of the droplet. The characteristics of temperature of the droplet follows a specific path throughout the whole drying process. However there may be differences according to properties and assumptions of the model. On the other hand as evaporation takes place, mass of the droplet is supposed to change because of continuous water loss. In previous sections change of mass of water in the droplet was presented, nevertheless comparison with literature is done with respect to overall mass of the droplet.

4.2.1. Comparison of Droplet Temperature

Farid [7] represented a clear illustration about different stages of drying of a liquid drop containing solid particles and accordingly the temperature profile of the droplet undergoing an evaporation process through those stages. Considering the whole process, as heating operation is initiated the droplet is supposed to heat until wet-bulb temperature of air before evaporation begins. As can be seen in Figure 4-14 [7], after the crust formation the temperature profile changes significantly, since until this point received heat is almost completely consumed by evaporation process just at the water interface, whereas recently formed crust begins to heat up afterwards as it is the region to receive the convective heat at first hand and conduct further to inner regions, hence increasing the temperature of the droplet.
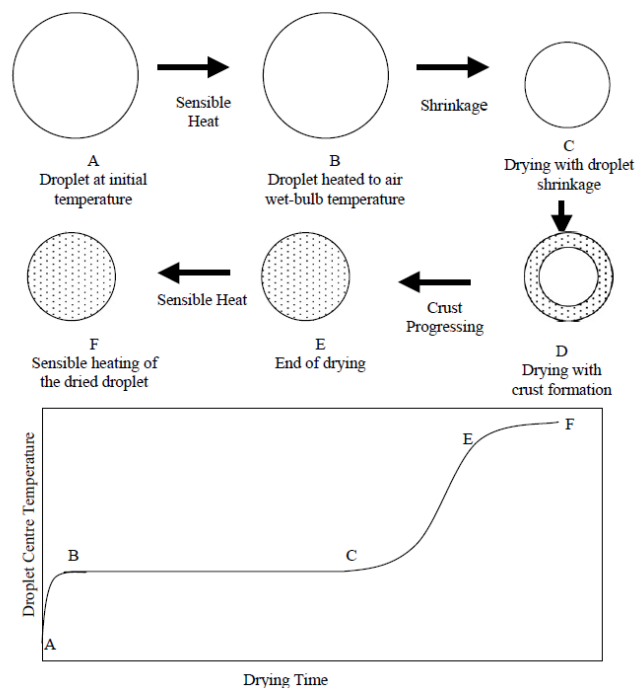

Figure 4.14. Stages of drying of a droplet with a common temperature profile

84

Regarding the overall temperature profile of a drying droplet, results of studied simulations in this thesis work are compared with corresponding regions of the plots, which are represented in various papers for the overall drying process. More specifically, the point indicated with C in above figure stands for the beginning of the second stage of drying, whereas point indicated with E represents the final time of drying. Thus, focus point of comparisons will be this region in illustrated temperature vs. time plots, basically matching the initial temperature data of the simulation to the temperature of point C.

Experimental and model results for drying a droplet containing colloidal silica are generally available for a couple of ambient temperature values, one of them being 101°C, which is the same temperature introduced intentionally in experimental comparison study. Comparison plots, which are represented in following pages, are generated by reading the approximate data from corresponding graphs, whose original illustrations are separately represented in Appendix D section for a more detailed look on request.

One of the papers, which is considered as a main reference belongs to Dalmaz [9] that utilized two numerical solution techniques in order to solve proposed model equations. In this paper overall drying process was investigated and compared with former literature data [6], whose comparison result is to be introduced subsequently. As mentioned in the discussion of initial study, an early sharp increase in temperature is observed for the simulation results, whereas temperature profile of the relevant paper demonstrates a constant trend along the drying process (see also Figure E-1). Apart from that, change in droplet temperature shows similar trends in both cases (Fig 4.15).
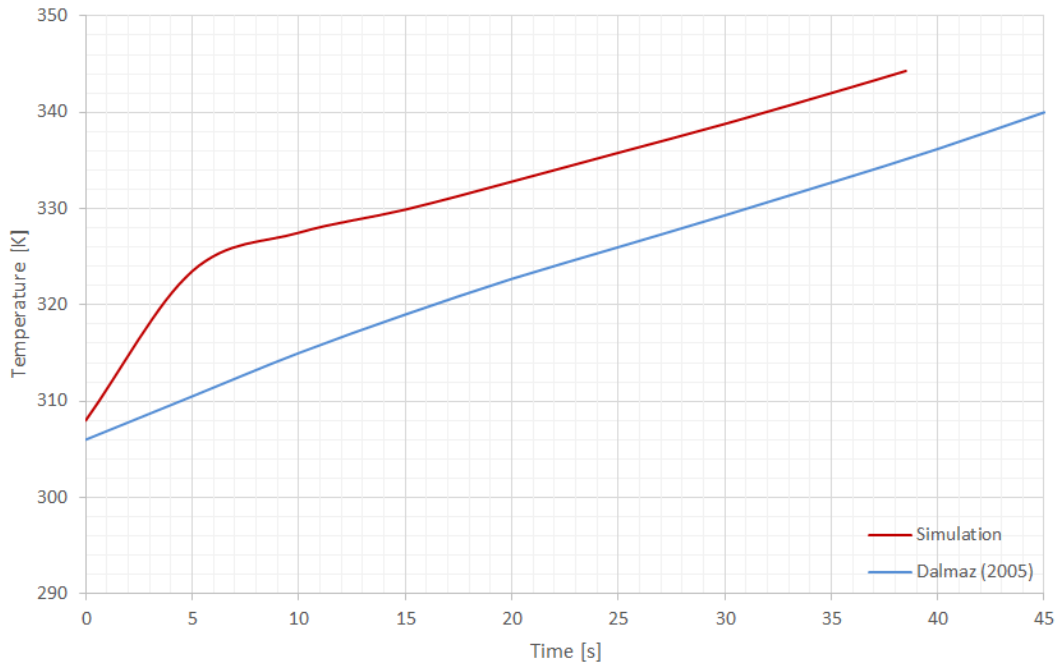
Figure 4.15. Comparison of temperature data of the simulation with relevant literature data-1

One of the reasons for a continuously constant increase trend of droplet temperature in the paper of Dalmaz [9] may be probably the constant morphology assumption taken into consideration in relevant study, causing the solid particles remain steady as the water interface recedes backwards. In this thesis work however, the solid particles form a crust region with high fraction, through which water vapor molecules diffuse slowly in initial seconds so that temperature increase of the droplet, particularly crust region, is relatively higher.

Experimental conditions presented in Nesic and Vodnik's paper [6] can be summarized as 101 °C air temperature, 1.73 m/s air velocity and 0.7 initial water fraction in the droplet. Except the particle fraction in the droplet, most of the conditions are assumed as the same in the simulation, as also mentioned in section 4.1.7. Since the initial

droplet diameter is 2.06 mm in the experiment, regarding the estimated amount of lost water in the first stage of the drying presented in Mezhericher's paper [1], an initial droplet diameter of 1.61 mm seems reasonable. Profiles similar to the experimental conditions can also be observed in other papers [13,14] where overall drying process is investigated at 101 °C. Temperature profiles of drying droplets are once again following the trend presented in Figure 4.14, thus current study results are compared with the relevant regions of figures given in mentioned papers, which are also available in Appendix section.
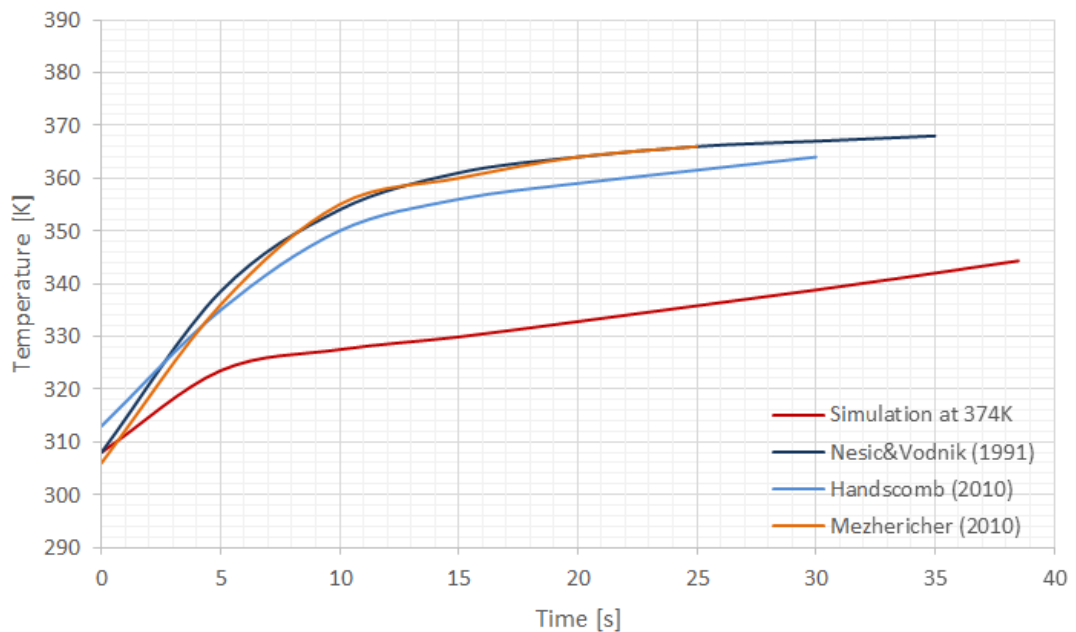

Figure 4.16. Comparison of temperature data of the simulation with relevant literature data-2

Temperature data from those papers are carefully read from original plots in order to keep accuracy of comparison at high levels. Main difference instantly attracting the attention of the observer is the initial increase amount in temperature of the droplet.

Although trend for temperature data show some differences but also intermediate agreement with other data (Fig 4.16).

As a reason for such difference in amount of temperature increase, two suggestions may be brought forward. Main cause is probably the mechanism introduced by proposed model, which prioritizes evaporation process, accordingly heat loss at evaporation interface, substantially. Thus, temperature increase of the droplet itself is limited as long as evaporation takes place. Secondarily, the aforementioned time interval following the initiation of simulation, in which droplet is heated up rapidly, lasts relatively shorter. Combining these two suggestions would provide a reasoning for appearing inconsistencies. Additionally in the next section, the change of mass data is plotted in comparison to other studies (Fig 4.18). Apparently, the drying process occurs relatively faster in the simulation, meaning that it requires more latent heat and leads to less temperature increase. On the other hand, initial water/solid fractions vary considerably between these studies, hence resulting in different average heat conductivities throughout the particle. Initial water fraction is assumed as 0.75 as a default value in the simulations, whereas that property shows an alteration in various literature data with an approximate value of 0.60. Since conductivity of solid material is roughly twofold of liquids', it is quite eventual to observe different regimes, because temperature profile of the droplet would demonstrate various trends for different volume fraction and ambient air values. It is also important to consider the fact that the experimental conditions may change throughout the process, for the water vapor layer just above the surface may create additional resistances as evaporation occurs, as well as humidity around the particle may show alteration. Recalling that these conditions are held constant in the simulation, aforementioned occurrences may be regarded as additional justifications for the discrepancy between the results.

Liming [17] presented experimental results of drying process of colloidal silica containing droplet at various temperatures. One of them is conducted at 65 °C, which is comparable with the initial study of the simulation run at 340 K. Although higher temperature experiments are also available in relevant paper, sufficient data for that particular case were already illustrated in Figure 4.16.
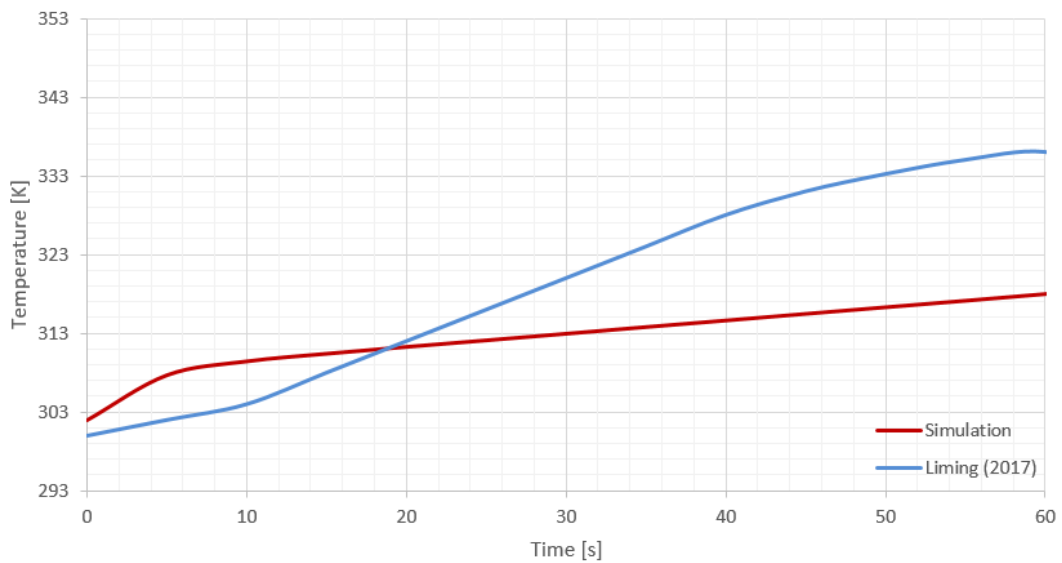

Figure 4.17. Comparison of temperature data of the simulation with relevant literature data-3

Initial heating of the particle seems to begin relatively slower in Liming's experimental work, therefore increase rate of temperature is low in early stages of second stage of drying. Nevertheless after some time temperature increases significantly, following a similar trend, which is already mentioned a couple of times. Since the time interval is shorter for the referenced plot, temperature profiles for relevant duration are plotted (Fig 4.17). Regardless of the short delay in temperature increase, temperature profile presented by Liming is similar to the ones in Figure 4.16. Thereby, similar reasonings may be discussed also for this particular case.

As a conclusion, the temperature profile of a nanosuspension droplet undergoing a complete drying process is quite definite. A plausible simulation is tried to be achieved with various assumptions specified for corresponding mechanisms and initial conditions. Because of discussed issues, a good agreement with literature data in terms of temperature profiles cannot be provided. However general trend of the simulation shows a reasonable similarity to compared temperature profiles.

4.2.2. Comparison of Droplet Mass

Mass of the droplet is supposed to decrease throughout the evaporation process. The rate of decrease in droplet mass is mainly determined by evaporation rate, whereas overall reduction percent depends on initial solid/water fraction. Although the experimental and model results available in the literature provide different mass amounts for various studies, an investigation of reduction in droplet mass by normalizing approach enables fine comparisons to be illustrated.

Below comparison is given for the change of droplet mass in numerical solutions of the models proposed by Nesic and Vodnik [6] and Dalmaz [9], compared to change of droplet mass estimated by the simulation, which is run at same conditions. Recall that only the data corresponding to the second stage of drying is scope of interest.
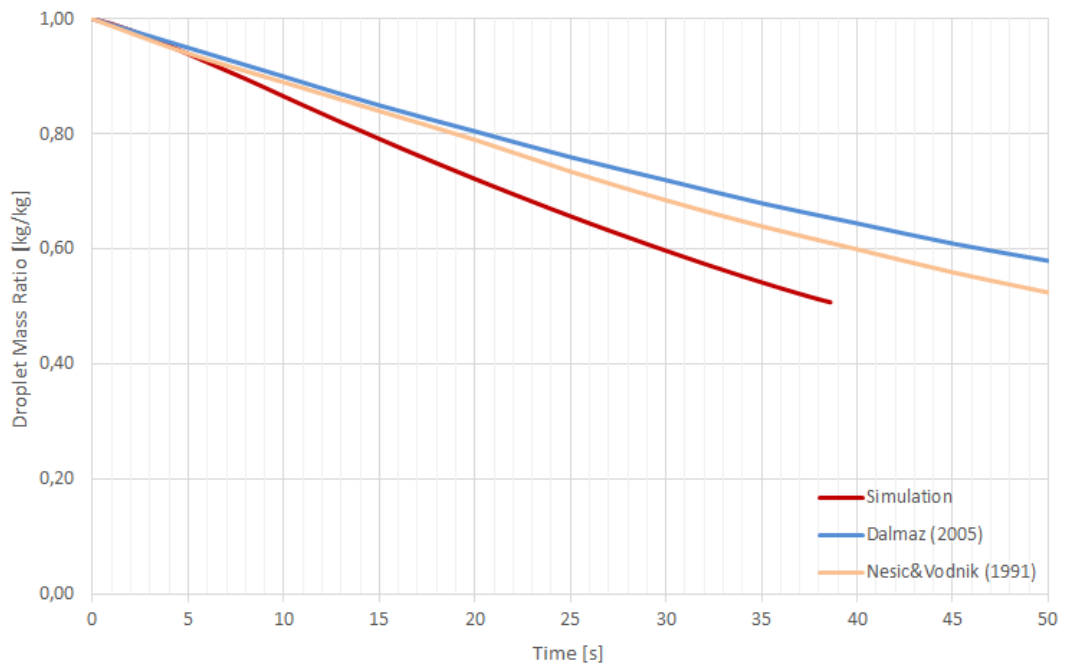
Figure 4.18. Comparison of droplet mass data of the simulation with relevant literature data-1

Figure 4.18 represents fairly good agreement in change of mass droplet with respect to time between the simulation results and relevant literature data. It seems that drying duration is shorter in the simulation whereas evaporation process lasts for a bit longer time in relevant examples (see Figure E-2). Eventually final droplet mass ratio ends up at a very close value, which is around 45-50%.

91

CHAPTER 5

CONCLUSION

The main purpose of the study is to present a model for both drying stages of a nanosuspension droplet and simulate the second stage via a computational program. Proposed model consists of partial differential equations describing heat and mass transfer mechanisms taking place throughout the drying process. The coupled equations are introduced into the simulation program, COMSOL, and solved simultaneously.

Drying operation is initially simulated with default conditions, of which some are referred from previous studies [9,1]. Initial study of the simulation involves drying air with temperature of 340 K, velocity of 0.5 m/s and absolute humidity of 0.01 g/g. The temperature of the droplet with an initial solid volume fraction of 0.25 is set to 302 K, as it is the corresponding wet-bulb temperature of air.

The simulation successfully estimated temperature and concentration histories of both liquid and gaseous regions in the particle with respect to time as well as position. From these results, the following conclusions may be drawn,

- The temperature of the particle initially increases rapidly then continues to increase relatively slower
- As the crust region thickens, resistance to heat transfer increases and evaporation rate falls slightly

- As water evaporates from the surface, water molecules tend to adhere the solid particles in the shell, eventually leaving a hollow region at the center

The simulation is run with different conditions, in which temperature, air velocity and humidity, and initial solid fraction and size of the droplet are varied. These studies lead to following conclusions,

- Increased air temperature significantly reduces the drying duration and increases heat transfer coefficient slightly because of high temperature properties of air.
- An increase in the velocity of ambient air also results in a reduced drying time, on the other hand increases the diffusion rate of water vapor molecules by increasing the mass transfer coefficient
- High relative humidity of air causes slower mass transfer for water vapor and consequently slower evaporation of water, resulting in longer drying time
- As the size of the droplet increases, drying time increases with a relatively higher ratio in comparison to the increase in droplet size, because of smaller surface to volume ratio of larger particles. However, temperature profile remains almost the same since most of the heat is lost by evaporation.
- Drying duration of the droplet is hardly affected by an increase in initial solid fraction. Although the formation of shell lasts longer because of high amount of solids, this delay is compensated by the time reduction provided by less amount of water to evaporate.

Although most of these conclusions are as expected and stating the obvious, the aim to prove both the model and the simulation are adjustable to yield accurate results for different conditions is fulfilled.

Additionally an experimental comparison study is conducted in order to make an accurate comparison with literature data, therefore the conditions of this study is arranged as substantially close to the conditions of various experiments and models in the literature. This comparison provides several outcomes to be reached such as,

- Temperature profile of the droplet shows similar trends with the results of the model proposed by Dalmaz [9], but fails to show good agreement with other relevant papers [6, 13, 14, 17]
- Change in droplet mass throughout the drying process shows fairly good agreement with profiles of both Dalmaz [9] and Nesic and Vodnik [6]

As a conclusion, this study has provided detailed results of the proposed model via a simulation program and it is anticipated that this thesis work will be beneficial for subsequent studies.

CHAPTER 6

RECOMMENDATIONS

There are several recommendations that can be suggested in order to further investigate the drying kinetics of a droplet containing solid particles. One of the main suggestions is that the simulation of the overall drying process can be studied with COMSOL in order to investigate the kinetics of both stages with the identical computational program. Apart from the results of proposed models in the literature, it would be also useful to investigate the results of the simulation beginning from the initial stage. Another recommendation is investigation of evolution of layer boundaries, such as shell boundaries and vacancy boundary. Additional work can be put into the studies about mechanisms like shell formation and vacancy emergence, since these incidents have critical roles throughout the morphological evolution of a drying droplet. As a final recommendation, although it has been out of the scope of this thesis, the conditions for ruptures and breakdown of the particle during the drying process can also be studied in detail.

REFERENCES

1. Mezhericher, M. et al., 2011. Modelling the Morphological Evolution of Nanosuspension Droplet in Constant-Rate Drying Stage, Chemical Engineering Science. 66, 884-896.

2. Ranz, W. E., Marshall, W. R., 1952. Evaporation from Drops. Chemical Engineering Progress. 48, 141.

3. Charlesworth, D. H., Marshall, W. R. Jr, 1960. Evaporation from Drops Containing Dissolved Solids. A.I.Ch.E. Journal, 6, 9-23.

4. Sano, Y., Keey, R. B., 1982. The Drying of a Spherical-particle Containing Collodial Material into a Hollow Sphere. Chemical Engineering Science. 37, 881

5. Cheong, H. W. et al., 1986. A Receding Interface Model for the Drying of Slurry Droplets. A.I.Ch.E. Journal. 32, 1334.

6. Nesic, S., Vodnik, J., 1991. Kinetics of Droplet Evaporation. Chemical Engineering Science. 46, 527-537.

7. Farid, M., 2003. A New Approach to Modelling of Single Droplet Drying. Chemical Engineering Science. 58, 2985-2993.

8. Seydel, P. et al., 2006. Modeling Particle Formation at Spray Drying Using Population Balances. Drying Technology. 24, 137-146.

9. Dalmaz, N. 2005. Modeling and Numerical Analysis of Single Droplet Drying. M.Sc. Thesis. Middle East Technical University, Ankara, Turkey.

10. Dalmaz, N. et al., 2007. Heat and Mass Transfer Mechanisms in Drying of a Suspension Droplet: A New Computational Model. Drying Technology. 25, 391-400.

11. Handscomb, C. S. et al. 2009. A New Model for the Drying of Droplets Containing Suspended Solids. Chemical Engineering Science. 64, 628-637.

12. Handscomb, C. S. et al. 2009. A New Model for the Drying of Droplets Containing Suspended Solids After Shell Formation. Chemical Engineering Science. 64, 228-246.

13. Handscomb, C. S., Kraft, M., 2010. Simulating the Structural Evolution of Droplets Following Shell Formation. Chemical Engineering Science. 65, 713-725.

14. Mezhericher, M. et al., 2007. Theoretical Drying Model of Single Droplets Containing Insoluble or Dissolved Solids. Drying Technology. 25:6, 1025-1032

15. Mezhericher, M. et al., 2008. Modelling of Particle Breakage during Drying. Science Direct. 47, 1404-1411.

16. Mezhericher, M. et al., 2008. Heat and Mass Transfer of Single Droplet/Wet Particle Drying. Chemical Engineering Science. 63, 12-13.

17. Liming, C. et al., 2017. Experimental Determination and Mathematical Modeling of the Drying Kinetics of a Single Droplet of Colloidal Silica. Drying Technology. 35:11, 1337-1346.

18. Tosun, I., 2013. The Thermodynamics of Phase and Reaction Equilibria. Elsevier.

19. Ochoa-Tapia, J. A. et al., 1994. Diffusive Transport in two-phase Media: Spatially Periodic Models and Maxwell's Theory for Isotropic and Anisotropic Systems. Chemical Engineering Science. 49, 709-726.

20. COMSOL, 2017. Heat Transfer Module User's Guide.

21. Millington, R. J., and J. P. Quirk, 1961. Transport in porous media. Trans. International Congress of Soil Science, 7(1), 97–106.

22. Rumpf, H., 1990. Particle Technology. Chapman and Hall, London.

23. Incropera, F. P., Dewitt, D. P., Bergman, T. L., Lavine, A. S., 2013. Foundations of Heat Transfer, Sixth Edition. Wiley.

APPENDICES

A. PROPERTIES OF MATERIALS

The materials used in simulation are water, silica, air and water vapor. The properties of water and water vapor are listed for 305K [23] for default case, since this temperature value is representing the approximate wet-bulb temperature of air for all conditions (see Appendix C). Additionally, throughout each individual study, these properties remain constant according to considered assumption, even though temperature changes occur. Properties of solid are presented for 300K [23], whereas properties of air are tabulated for two different temperature values, which are 330K and 350K. [23] The essential criterion for choosing these temperature values are that an average value of film temperature (droplet boundary) and ambient temperature is considered. If a certain property value is taken from an article, it is specified with corresponding reference.

Table A.1. *Properties of water*

Property	Abbreviation	Unit	at 305K
Density	ρ_w	kg/m^3	*995*
Molecular Weight	M_w	kg/mol	*1.802x10^{-2}*
Heat Capacity	cp_w	kJ/kgK	*4.178*
Heat Conductivity	k_w	W/mK	*0.620*
Latent Heat of Vaporization	λ_w	kJ/kg	*2426*
Diffusivity [1]	D_w	m^2/s	*10^{-7}*

Table A.2. *Properties of water vapor*

Property	Abbreviation	Unit	at 305K
Density	ρ_{wv}	kg/m^3	*0.0336*
Heat Capacity	cp_{wv}	kJ/kgK	*1.877*
Diffusivity [9]	D_{wv}	m^2/s	*2.67x10^{-5}*
Heat Conductivity	k_{wv}	W/mK	*2.01x10^{-2}*

Table A.3. *Properties of air*

Property	Abbreviation	Unit	at 330K	at 350K
Density	ρ_a	kg/m^3	*1.09*	*0.995*
Heat Capacity	cp_a	kJ/kgK	*1.008*	*1.009*
Viscosity	μ_a	Ns/m^2	*1.94x10^{-5}*	*2.08x10^{-5}*
Heat Conductivity	k_a	W/mK	*2.78 x10^{-2}*	*3.00 x10^{-2}*

Table A.4. *Properties of silica*

Property	Abbreviation	Unit	at 300K
Molecular Weight	M_s	kg/mol	*6.009 x10^{-2}*
Density	ρ_s	kg/m^3	*2220*
Heat Capacity	cp_s	kJ/kgK	*0.745*
Heat Conductivity	k_s	W/mK	*1.38*

Table A.5. *Properties of water vapor in crust region*

Property	Abbreviation	Unit	at 305K
Diffusivity [19]	D_{cr}	m^2/s	*8.21x10^{-6}*
Heat Conductivity	k_v or k_{mix}	W/mK	*2.39x10^{-2}*

B. GENERAL PARAMETERS FOR SIMULATION

There are several parameters introduced into simulation program that determines general conditions of the setup.

Table B.1. *General parameters for simulation*

Property	Abbreviation	Unit	Default values
Ambient Temperature	T_0	K	*302*
Pressure	P	atm	*1.0*
Air Temperature	T_a	K	*340*
Air Velocity	v_a	m/s	*0.5*
Absolute Humidity	AH	g/g air	*0.01*
Shell and Crust Porosity	ε	-	*0.40*
Slurry Porosity	φ_w	-	*0.75*

Moreover, coefficients for mass and convective heat transfer operations are estimated. Although convective heat transfer coefficient is automatically calculated by the simulation program instead of introducing a beforehand calculated value, it is presented for informative purposes.

$$k_m = 2\frac{D_{wv}}{d_p} + 0.65 \left(\frac{v_a}{d_p}\right)^{0.5} \left(\frac{\rho_a}{\mu_a}\right)^{0.17} D_{wv}{}^{0.67} \tag{3.27}$$

$$k_m = 2\frac{2.67 \times 10^{-5}}{1.61 \times 10^{-3}} + 0.65 \left(\frac{0.5}{1.61 \times 10^{-3}}\right)^{0.5} \left(\frac{1.09}{1.94 \times 10^{-5}}\right)^{0.17} (2.67 \times 10^{-5})^{0.67} = 0.097\frac{m}{s}$$

$$h = 2\frac{k_a}{d_p} + 0.65 \left(\frac{v_a \rho_a}{d_p}\right)^{0.5} k_a{}^{0.67} cp_a{}^{0.33} \mu_a{}^{-0.17} \qquad (3.18)$$

$$h = 2\frac{2.78 \times 10^{-2}}{1.61 \times 10^{-3}} + 0.65 \left(\frac{(0.5)(1.09)}{1.61 \times 10^{-3}}\right)^{0.5} (2.78 \times 10^{-2})^{0.67}(1.008)^{0.33}(1.94 \times 10^{-5})^{-0.17} = 41.41\ \frac{W}{m^2 K}$$

Value of the coefficients are also tabulated below for the conditions in different studies.

Table B.2. *Heat and mass transfer coefficients for different studies*

Property	Unit	Initial Study	Increased T_a	Increased v_a	Increased R_d
Heat Transfer Coefficient, h	W/m²K	*41.41*	*44.10*	*44.26*	*22.13*
Mass Transfer Coefficients, k_m	m/s	*0.097*	*0.095*	*0.123*	*0.061*

C. PSYCHROMETRIC PROPERTIES

Wet-bulb temperature of air is determined for corresponding humidity ratios and dry-bulb temperatures of air according to the psychrometric charts and calculators online. Additionally, percent of relative humidity in ambient air are tabulated for initial, increased temperature and increased humidity cases.

Table C.1. *Psychrometric properties*

Dry Bulb T of Air	Absolute Humidity	Wet Bulb T of Air	Relative Humidity
340K	0.01	302.2 K	5.8%
370K	0.01	307.8 K	1.8%
340K	0.02	306.8 K	11.3%

D. REFERENCED PLOTS FROM LITERATURE

Comparison of the results are done with relevant data plotted in previous articles. In this section, the plots from corresponding papers are represented in order to provide an opportunity to view original figures.
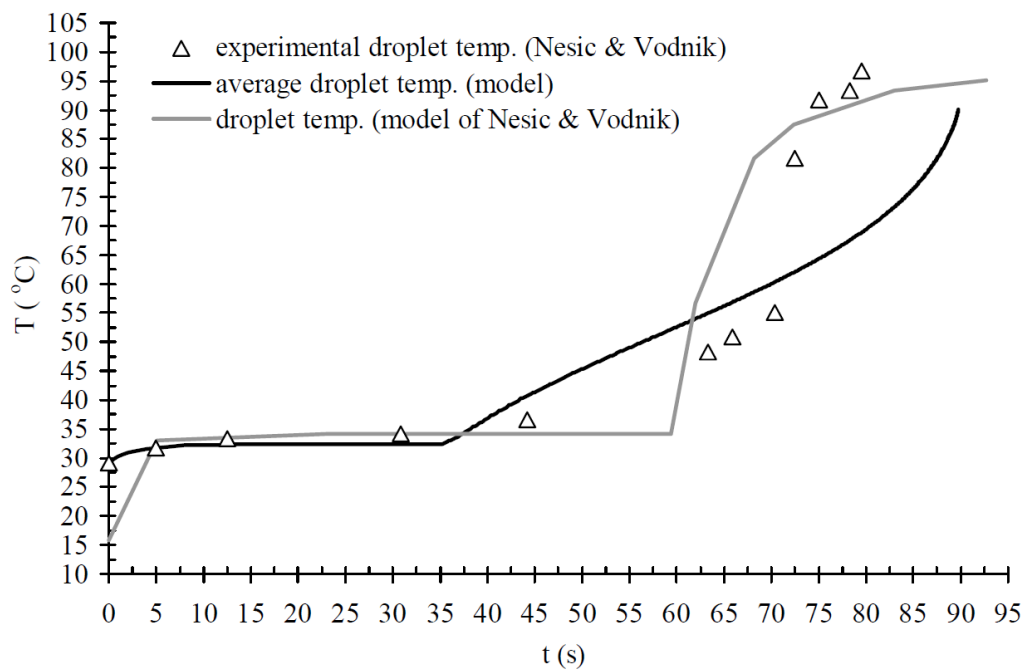

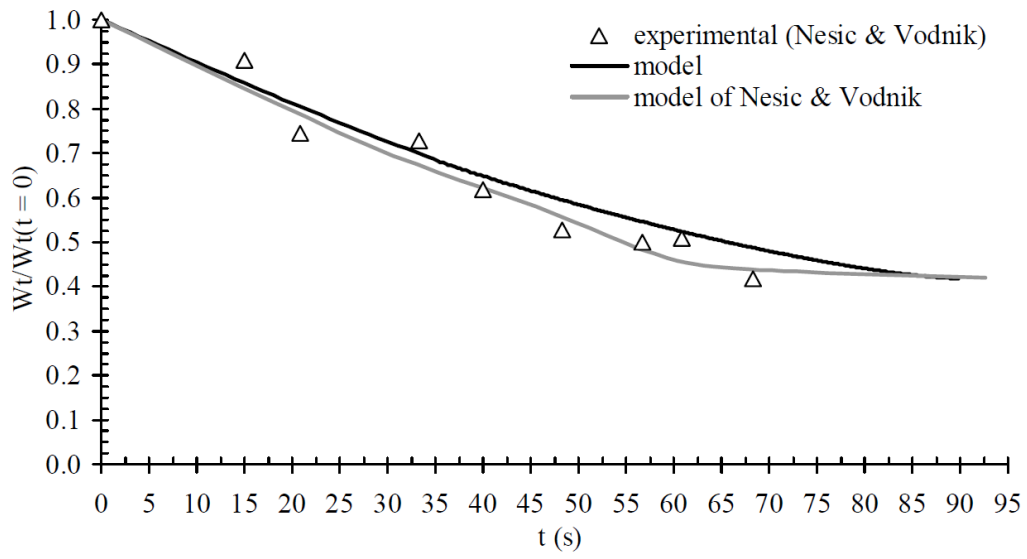*Figure D.1*. Temperature data represented in articles 6 and 9

107

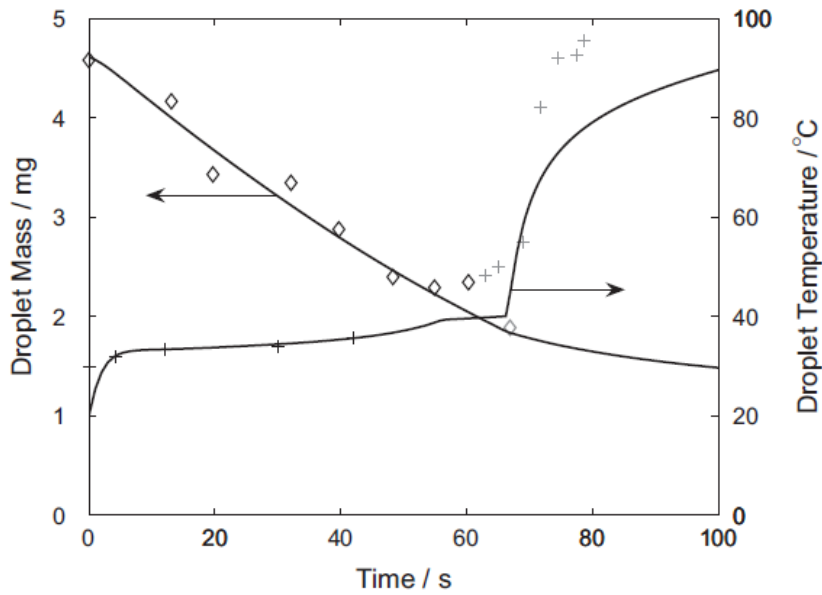*Figure D.2.* Change of droplet mass data represented in articles 6 and 9

Figure D.3. Temperature and mass data represented in article 13
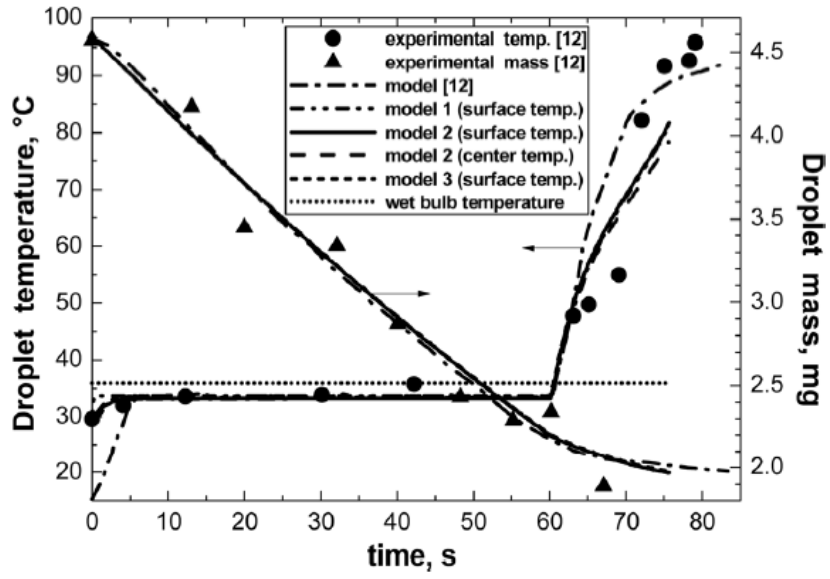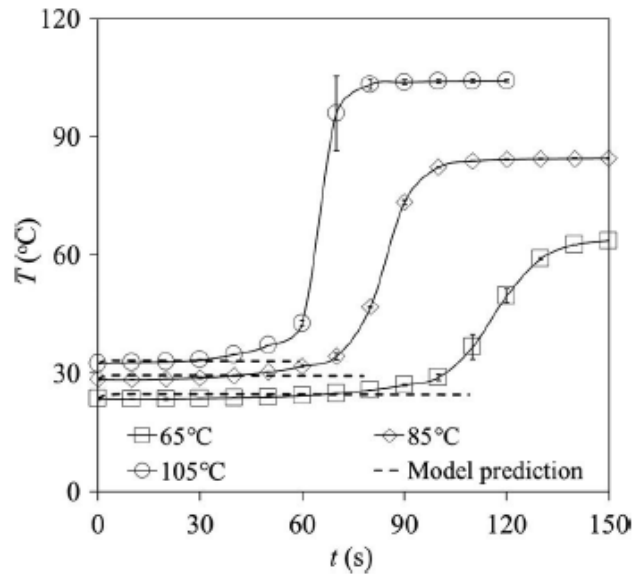
108

Figure D.4. Temperature and mass data represented in article 14

Figure D.5. Temperature data represented in article 17